THE WIP6 TRANSCRIPTION FACTOR *TOO MANY LATERALS* SPECIFIES VEIN TYPE IN C_4 AND C_3 GRASS LEAVES

Daniela Vlad, Maricris Zaidem, Chiara Perico, Olga Sedelnikova[1], Samik Bhattacharya[2], & Jane A. Langdale*

Department of Biology, University of Oxford, South Parks Rd, Oxford, OX1 3RB, UK

[1] Current address: Syngenta Jealott's Hill International Research Centre, Bracknell RG42 6EY, UK

[2] Resolve BioSciences GmbH, Alfred-Nobel-Straße 10, 40789 Monheim am Rhein, Germany

*Author for correspondence: jane.langdale@biology.ox.ac.uk

ABSTRACT

Grass leaves are invariantly strap shaped with an elongated distal blade and a proximal sheath that wraps around the stem. Underpinning this uniform shape is a scaffold of leaf veins, most of which extend in parallel lines along the proximo-distal leaf axis. Differences between species are apparent both in the types of veins that develop and in the spacing between them across the medio-lateral leaf axis. A prominent engineering goal is to increase vein density and the proportion of bundle sheath cells surrounding the veins in leaves of C_3 photosynthesizing species such as rice, in order to facilitate introduction of the more efficient C_4 photosynthetic pathway. Here we discover that the WIP6 zinc finger transcription factor TOO MANY LATERALS (TML) specifies vein rank in both maize (C_4) and rice (C_3), species with distinct venation patterns. Loss of function *tml* mutations lead to the development of large lateral veins in positions normally occupied by smaller intermediate veins. The spatial localization of *TML* transcripts in wild-type leaves is consistent with a role in suppressing lateral vein formation in procambial cells that develop intermediate veins, specifically the class of intermediate veins that extend from the leaf blade into the leaf sheath. Attempts to manipulate TML function in rice were unsuccessful because transgene expression was silenced, suggesting that precise spatial and temporal regulation of *TML* expression is essential during the regeneration of shoot tissue from callus. Given that transcriptome analysis demonstrated altered profiles of genes associated with cytokinin and auxin signaling in loss of function maize mutants, the necessity for tight regulation of *TML* gene expression could be an indirect consequence of hormonal inbalances as opposed to ectopic activity of a specific downstream target. Importantly, however, loss of function mutants in rice display increased vascular and bundle sheath cell occupancy in the leaf. Collectively this work provides an understanding of how vein rank is specified in grass leaves and a first step towards an anatomical chassis for C_4 engineering in rice.

KEYWORDS: leaf development; maize; rice; vein patterning; WIP proteins

INTRODUCTION

Biological patterns form during the development of multicellular organisms when cell fates are mapped onto fields of equivalent pluripotent cells in organized space and time [1]. In flowering plants, patterning primarily occurs post-embryogenesis at the shoot and root apical meristems, with shoot patterns most obvious in the geometrical arrangement of leaves around the apex and in floral morphologies [2]. Less obvious is the patterning of veins within leaves, which in flowering plants is of two distinct types. In eudicotyledonous (eudicot) plants, leaf veins form reticulated networks whereas in monocotyledonous (monocot) plants, veins run in parallel along the length of the proximo-distal leaf axis (reviewed in [3,4,5]). Both the reticulate venation pattern in eudicot leaves and the striated pattern in monocot leaves result from the organized specification of vein-forming stem cells (procambial initial cells) within the ground meristem of the leaf [6], with temporal regulation facilitating the sequential formation of different vein ranks and spatial regulation defining the distance between veins.

Vein patterning mechanisms are best characterized in eudicots where the regulated flux of auxin determines the direction and extent of vein development. In the eudicot *Arabidopsis thaliana* (Arabidopsis), auxin flux occurs both via passive diffusion through plasmodesmata [7] and active transport through membrane localized transporters [8,9], with the asymmetric distribution of efflux carriers such as PIN FORMED1 (PIN1) directing flux from the leaf margin to the midvein through narrow strands of procambium (reviewed in [10]). The specification of procambial initials (referred to as preprocambial cells in Arabidopsis [11]) that form the procambial strands occurs when auxin signaling activates the expression of the auxin response factor *MONOPTEROS/ARF5* (*MP*) [12]. MP then elevates PIN1 expression in a feedback loop and induces expression of the HD-ZIP III transcription factor *ARABIDOPSIS THALIANA HOMEOBOX 8* (*ATHB8*), which marks procambium identity and stabilizes PIN1 localization [13]. The PIN/MP/ATHB8 module thus reinforces auxin flux and leads to the extension of procambial strands. Although procambium develops simultaneously along a file of preprocambial cells, it is important to note that veins form sequentially in rank order with new procambial strands developing towards, and connecting with, those that have already formed [14,15].

Little is known about vein patterning in monocot leaves but mechanisms appear inherently different from those in eudicots because successive vein ranks are positioned in between and parallel to existing veins, with connections only made late in development when transverse veins form across the medio-lateral leaf axis. Vein ontogeny in monocots is best characterized in grasses such as *Zea mays* (maize) where four longitudinal vein ranks develop [16,17]. The midvein develops first, differentiating from the base of the leaf primordium to the tip, the lateral veins develop next (also towards the leaf tip) and then the rank 1 and rank 2 intermediate veins develop in turn from the tip towards the base. Only the largest of the rank 1 veins, which are associated with sclerenchyma on both the adaxial and abaxial sides, extend into the leaf sheath and as such the veins in the sheath are spaced further apart than those in the blade. In maize, the four longitudinal vein ranks underpin a cellular arrangement known as Kranz

anatomy in which each vein is surrounded by concentric rings of photosynthetic bundle sheath cells and mesophyll cells, and all veins in the blade are separated by just four cells in the medio-lateral leaf axis (reviewed in [18]). This anatomy, which is associated with C_4 photosynthesis, evolved on multiple independent occasions from the ancestral anatomy found in C_3 photosynthesising grasses such as *Oryza sativa* (rice) [19]. In C_3 grass leaves, rank 2 intermediate veins are absent and vein pairs in the blade are separated by up to ten mesophyll cells. Venation patterns in C_4 grass leaves therefore differ from those in C_3 grasses, both in terms of the spacing between veins (closer in C_4 than C_3) and in the number of vein ranks (more in C_4 than C_3) (reviewed in [3]). In both C_4 and C_3 leaves, however, the timing of vein initiation is similar. The midvein initiates at plastochron (P) 1 (where a plastochron is the time interval between initiation of primordia at the meristem and P1 is the most recently formed), the laterals at P2/P3 and the intermediates between P3 and P5 [16,20,21]. In each case, as in eudicots, cells in procambial strands are marked by expression of a *PIN* gene [22-25] but the strands are not directed towards existing veins, suggesting that the spacing of veins across the medio-lateral leaf axis is pre-patterned within ground meristem cells of the emerging primordium. With the exception of the homeobox gene *OsHOX1,* which is expressed in procambial cells of developing rice leaf primordia [26], the identity of genes acting downstream of auxin during the formation and extension of procambial strands in monocot leaves remains elusive.

Here we identify a gene encoding a WIP C2H2 zinc finger protein [27] that is expressed in procambial initial cells in the leaves of multiple grass species. The maize gene Zm00001d020037 (B73 v3 - GRMZM2G150011; B73 v5 - Zm00001eb309530) was first identified as a candidate regulator of vein patterning in a transcriptome analysis of maize foliar and husk leaf primordia [28]. Transcript accumulation profiles from P1 to P5 indicated an increase in expression levels prior to the initiation of veins in developing P1/P2 primordia and a decrease after P5 once all veins had been specified. The gene was hypothesized to be a regulator of Kranz anatomy [29]. Through loss of function analyses in maize and *Setaria viridis* we demonstrate that the WIP6 gene *TOO MANY LATERALS* (*TML)* facilitates development of the correct ratio of lateral to intermediate veins in C_4 grass leaves. Rather than being specific for Kranz anatomy, however, we show that aspects of TML function are conserved between C_4 and C_3 species, enabling venation patterns to be modified in rice.

RESULTS

A canonical EAR domain is present in monocot but not eudicot WIP6 proteins

As a first step towards understanding the likely function of the maize gene Zm00001d020037, orthologous genes were identified in predicted proteomes of all species using Orthofinder [30] (**Supplementary File 1**). The orthogroup contains WIP proteins, which are specific to land plants and are characterized by a conserved three amino acid 'WIP' sequence and four zinc finger domains [31]. Phylogenetic inference revealed a single gene in the bryophyte *Marchantia polymorpha* (*MpWIP*), evidence of a gene duplication that generated WIP6 and a second clade in the last common ancestor of vascular plants, and further duplications in the last common ancestor of the flowering plants which

142 subdivided the second clade into WIP1, WIP3 and WIP2/4/5 clades (**Figure 1A, Supplementary Files**
143 **2 & 3**). Zm00001d020037 and its paralog Zm00001d005566 are members of the WIP6 clade. The only
144 gene in this clade for which function has been reported is Arabidopsis *WIP6,* which was named
145 *DEFECTIVELY ORGANISED TRIBUTARIES 5* (*DOT5*) on the basis of leaf venation defects observed
146 in a T-DNA insertion line [32]. However, recent work refuted a role for *AtWIP6* in venation patterning,
147 being unable to identify any developmental perturbations in loss of function mutants created by gene
148 editing [33,34]. As such, in the absence of a known function, we initially named the maize genes *ZmWIP6A*
149 (Zm00001d020037) and *ZmWIP6B* (Zm00001d005566).
150
151 Within the WIP6 clade, eudicot and monocot sequences form two discrete sub-clades (**Figure 1A, 1B,**
152 **& S1A, Supplementary Files 4-6**). In the monocot clade, with the exception of maize, most genomes
153 contain a single copy of WIP6 as seen in the basal monocots *Zostera marina* and *Spirodela polyrhiza*.
154 In maize, *ZmWIP6A* (chromosome 7) and *ZmWIP6B* (chromosome 2) are not in syntenic regions of
155 the genome [35] and are thus unlikely to have arisen from the whole genome duplication event that
156 generated many homeologous genes in the species. A protein alignment of 50 predicted WIP6 protein
157 sequences from 41 species highlights the WIP sequence plus the four highly conserved zinc finger
158 domains arranged in tandem at the C terminus [27,31,36] (**Figure 1C, Figure S1B, Supplementary File**
159 **7**). Towards the N terminus, a putative EAR motif (LxLxPP) [37] is present in both eudicot and bryophyte
160 proteins but only the monocot proteins contain a *bona fide* LxLxL-type EAR motif [38]. Given that LxLxL
161 EAR motifs are known to mediate transcriptional repression of target genes [37], the observed
162 monocot/eudicot differences in this region could reflect a repressor role for WIP6 proteins specifically
163 in monocots.
164
165 ***WIP6* gene transcripts accumulate in procambial cells that will form intermediate veins in grass**
166 **leaf primordia**
167 In the context of whole leaf primordia, transcripts of both *ZmWIP6A* and *ZmWIP6B* accumulate to
168 relatively low levels (550 and 80 transcripts per million respectively [28]), but expression analyses at the
169 whole tissue level can mask big differences between individual cells within the tissue. To evaluate the
170 spatial pattern of *ZmWIP6A* and *ZmWIP6B* expression, *in situ* hybridization experiments were
171 performed with sections of maize shoot apices that included late P2-5 leaf primordia. For orientation,
172 Figure 2A depicts a schematic of a P4 leaf primordium showing the position of procambial initial cells
173 and of procambial centres (dividing procambial cells that will give rise to veins), and Figure 2B shows
174 a schematic of lateral and intermediate veins in an expanded leaf. Transcripts were detected in
175 developing procambial centres of P3, P4 and P5 primordia, with *ZmWIP6A* accumulating to higher
176 levels than *ZmWIP6B* in the leaf blade (as seen in transcriptomic experiments) (**Figure 2C, 2D**). The
177 presence of veins at different stages of development in each leaf primordium further revealed the
178 temporal pattern of *ZmWIP6* expression, with transcripts present in the single procambial initial cell
179 and in the first four or five derivatives of that cell during the initation of intermediate veins but absent at
180 later stages of development (**Figure 2E**). Similar spatial expression profiles were seen in other grass

181 species examined, with expression of the single WIP6 ortholog in each case being confined to
182 developing veins in *Setaria viridis*, *Sorghum bicolor* and rice primordia (**Figure S2A-C**). In rice,
183 however, where veins are initiated further apart than in the three other species, the temporal profile of
184 *OsWIP6* expression differs in that transcripts are detectable at later stages of vein development than
185 seen in maize (**Figure S2D**). Collectively, these data suggest that WIP6 orthologs may play a role in
186 the specification of procambial initial cells within the ground meristem of developing leaf primordia in
187 both C_4 and C_3 species.
188
189 To gain a more precise understanding of the spatial and temporal expression profile of *ZmWIP6* genes,
190 and to also examine transcript accumulation patterns in the shoot apical meristem plus P0 and P1 leaf
191 primordia, fragments of both genes were hybridized to sections of maize shoot apices using Resolve
192 Biosciences Molecular Cartography technology. The ability to visualize individual cells and to
193 simultaneously quantify transcripts of both genes within them revealed an overlapping but distinct
194 expression pattern for each gene. Specifically, *ZmWIP6A* is expressed in developing intermediate
195 veins of all leaf primordia examined, whereas *ZmWIP6B* is only expressed in a subset (**Figure 2D, E**).
196 Neither gene is expressed in the midvein or lateral veins at any stage of development. (Note that
197 although some signal was detected in the early P2 primordium where intermediate veins have yet to
198 be initated, the signal was not localized to procambial centres). Co-localization of *ZmWIP6A* and
199 *ZmWIP6B* transcripts is most apparent in developing intermediate veins of the P5 primordium (arrows
200 in **Figure 2E & Figure S2**). In this regard it is important to note that a transverse section across the
201 shoot apex captures leaf primordia at different positions along their proximo-distal axes. In this case,
202 the P1 section is at the very tip of the blade, P2 and P3 are near the middle of the blade, P4 is at the
203 base of the blade and P5 is in the leaf sheath. Given that intermediate vein development in the leaf
204 sheath is the last stage of vein patterning within any grass leaf primordium, these observations suggest
205 that *ZmWIP6A* may be required from the earliest stages of intermediate vein formation whereas
206 *ZmWIP6B* function may only be required either late in development or specifically in the leaf sheath.
207 Intriguingly, although *ZmWIP6A* activity appears to be restricted to the first few divisions in procambial
208 centres of P3-P5 primordia, transcripts are also detected at later stages of development, alongside
209 *ZmWIP6B* around mature veins in the leaf sheath. These observations suggest that *ZmWIP6A* may
210 have a non-redundant specification role early in development of the leaf blade and a redundant role
211 with *ZmWIP6B* later in the development of the leaf sheath.
212
213 **Loss of function *Zmwip6A* mutants develop too many lateral veins**
214 To determine whether *ZmWIP6A* or *ZmWIP6B* expression patterns reflect a role in leaf venation
215 patterning, loss of function alleles were generated by CRISPR/Cas9 mediated gene editing. Two guide
216 RNA sequences (sgRNAs) were designed to target each gene at sites flanking the EAR domain
217 (**Figure 3A**) and all four sgRNAs were assembled into a single construct for transformation into the
218 maize inbred line B104. Resultant T0 plants were backcrossed to B104 and four T1 lines representing
219 different combinations of mutant alleles were obtained (**Figure 3B**). One line contained mutations in

220 *ZmWIP6A,* one in *ZmWIP6B,* and two in both genes. Within the four lines, there were four independent
221 alleles of *ZmWIP6A* and three of *ZmWIP6B*, with one of the double mutant lines (438_I20) being
222 heteroallelic at both loci. For *ZmWIP6A*, one of the mutant alleles (I20_3) encoded an almost full-length
223 protein with just five amino acids deleted upstream of the EAR domain (**Figure S3A**). No further
224 characterization was carried out with this allele (*Zmwip6A_m4*) because the encoded protein was likely
225 to be at least partially functional. The remaining three *ZmWIP6A* alleles contained a 268 bp deletion
226 (J3) or single base pair insertions (B1_10 & I20_18) that resulted in premature stop codons upstream
227 of the zinc finger domain and thus represented loss of function alleles (**Figure S3A**). These alleles
228 were named *Zmwip6A_m1* (J3), *Zmwip6A_m2* (B1-10) and *Zmwip6A_m3* (I20_18). For *ZmWIP6B,* a
229 281 bp deletion that resulted in a premature stop codon in line J3 was named *ZmWIP6B_m1.* Two
230 further alleles were isolated from line 438_I20. One contained a 286 bp deletion (*Zmwip6B_m2*) and
231 the second contained a 3 bp deletion plus a single bp insertion (*Zmwip6B_m3*) (**Figure S3B**). Both
232 result in the formation of premature stop codons and predicted loss of gene function. Homozygous
233 mutations that had segregated independently from the transgene were identified in progeny of the six
234 self-pollinated T1 lines and single and double combinations of mutant alleles were fixed for phenotypic
235 characterization.
236
237 To assess the phenotypic impact of loss of ZmWIP6 function, single and double mutant plants were
238 grown alongside null segregants. None of the mutants exhibited general growth perturbations (**Figure**
239 **S3C-F**), although *Zmwip6A_m2* mutants sometimes developed male inflorescences (tassels) with
240 fewer fertile spikelets than segregating wild-type plants. In leaves, venation patterns were perturbed in
241 single *Zmwip6A* mutants and in double mutants, but not in single *Zmwip6B* mutants (**Figure 3C**).
242 Specifically, *Zmwip6A* and *Zmwip6A;Zmwip6B* mutant leaves developed twice as many lateral veins
243 than corresponding wild-type siblings, with a concomitant decrease in the number of intermediate veins
244 (predominantly rank 1 intermediates with sclerenchyma on both the adaxial and abaxial sides) (**Figure**
245 **3D**). Notably, the same phenotype was observed in leaves of *S. viridis* when the single *SvWIP6* gene
246 was edited (**Figure S3C-F**). Given that the number of ectopic lateral veins was the same in single
247 *Zmwip6A* mutants as in double mutants, no role could be inferred for *ZmWIP6B* in the regulation of
248 vein type. When total vein number across the medio-lateral axis was quantified, however, *Zmwip6B*
249 mutants were indistinguishable from wild-type but the two double mutants that were analyzed had
250 fewer veins than single *Zmwip6A* mutants (**Figure 3E**). We thus conclude that *ZmWIP6B* plays a minor
251 (as yet unidentified) role in venation patterning compared to *ZmWIP6A*. On the basis of the mutant
252 phenotypes, we renamed the *ZmWIP6A* and *ZmWIP6B* genes *TOO MANY LATERALS* (*ZmTML1* &
253 *ZmTML2*) and because of the conserved mutant phenotype, the *S. viridis* ortholog was named *SvTML*.
254
255 The development of extra lateral veins in *Zmtml1* mutants could result from the specification of
256 additional lateral veins or from mis-specification of intermediate veins. To distinguish these possibilities,
257 transverse sections of P4 primordia were examined at the base and middle of the primordium (**Figure**
258 **3F-I**). If the extra lateral veins result from ectopic specification, more laterals would be visible at the

259 base of mutant P4 primordia than in null sgregants, because lateral veins differentiate from base to tip
260 and are specified by P4. By contrast if the phenotype results from mis-specification of intermediate
261 veins, developing veins sited in between lateral veins in the middle of mutant P4 primordia would be
262 larger (more lateral-like) than in null segregants, because intermediate veins develop from tip to base
263 and at P4 they are more differentiated in the middle than the base of the leaf. **Figures 3F, 3G** show
264 that the number of lateral veins at the base of the P4 primordium is the same in null segregant and
265 mutant samples. Developing veins positioned between the laterals look slightly larger in the mutant
266 than in the null segregant but in both cases they are smaller than the adjacent lateral veins.
267 Comparisons between **Figure 3H** and **3I**, however, reveal more veins with lateral identity in the middle
268 of mutant primordia than in null segregants. Because ectopic lateral vein identity is evident in the middle
269 but not the base of the primordium, we conclude that the mutant phenotype arises as a consequence
270 of mis-specification of basipetally differentiating intermediate veins as lateral veins. This conclusion is
271 validated because the rank 1 intermediate veins that differentiate from the tip of the blade into the
272 sheath are clearly distinguishable from adjacent lateral veins in null segregants, but in mutant leaves
273 they are not (**Figure 3J, K**). Notably, these longitudinal images also revealed no differences between
274 mutants and null segregants in the pattern of transverse veins connecting lateral and intermediate
275 veins across the medio-lateral leaf axis (**Figure 3J, K**). During wild-type development ZmTML1 must
276 therefore act to suppress lateral vein identity in procambial centres that form rank 1 intermediate veins,
277 specifically those rank 1 veins that are associated with sclerenchyma on both the adaxial and abaxial
278 sides and extend from the leaf blade into the leaf sheath.
279
280 **Transcriptomes suggest altered cell division dynamics and auxin responses in *Zmtml1tml2***
281 **mutants.**
282 To identify potential targets of *ZmTML* function during early leaf development and to assess which
283 processes are perturbed in mutant leaves, transcriptome profiles were compared between shoot apices
284 (comprised of the shoot apical meristem and P1-P5 leaf primordia) of double *Zmtml1tml2* mutants and
285 segregating wild-type siblings. Transcripts were quantified to identify those where levels showed a
286 significant difference (log 2-fold change (L2FC) > 1; $p < 0.05$) between wild-type and mutant
287 (**Supplementary File 8**). (All fold differences referred to below are L2FC at $p < 0.05$). Levels of
288 transcripts encoded by 591 genes were significantly higher in mutant samples than wild-type and those
289 encoded by 1275 genes were lower. GO term enrichment analysis of these 1866 genes revealed a
290 broad range of functions that are perturbed in mutant plants, with those encoding transcription factors
291 notably enriched for terms associated with shoot apical meristem development and adaxial/abaxial
292 axis specification (**Figure 4A**). 89 transcripts representing 47 genes were up-regulated greater than
293 20-fold in the mutant, with the majority encoding enzymes or structural proteins (**Supplementary File**
294 **8**). By contrast, 45 transcripts representing 24 genes were down-regulated greater than 20-fold in the
295 mutant and of the 11 genes in that group that have been annotated, 5 encode proteins that regulate
296 gene activity (e.g. through ubiquitination, histone acetylation, histone methylation, chromatin
297 remodelling or RNA silencing) (**Supplementary File 8**).

298 Of the few genes directly implicated in the development of Kranz anatomy (*SHORTROOT (SHR)* [39],
299 *SCARECROW (SCR & SCR1h)* [40-42] and *NAKED ENDOSPERM (NKD1 & NKD2)* [43], only *NKD2*
300 transcript levels were significantly different between mutant and wild-type (lower in the mutant - L2FC
301 = 1; $p < 0.05$) (**Supplementary File 9**) suggesting that *ZmTML* genes act downstream of any 'Kranz
302 patterning module'. Notably, the failure to detect differences in levels of transcripts encoding orthologs
303 of procambial markers in Arabidopsis (*ATHB8/ZmHB52* and *PIN1*) and rice (*OsHOX1/ZmHB78*)
304 (**Supplementary File 9**) could also suggest that ZmTML function is downstream of procambium initial
305 cell specification. The development of normal vein numbers in loss of function *Zmtml1tml2* mutants
306 (**Figure 3D, E**) would also support this suggestion. However, *ZmHB52* is expressed more broadly than
307 *ZmTML1* in wild-type leaf primordia, with transcripts detected across the P1 leaf primordium and in the
308 more actively dividing cells at the margins of older primordia (**Figure S4A, S4B**). Restriction of *ZmHB52*
309 transcripts to dividing procambial centres only occurs after *ZmTML1* transcript accumulation is
310 repressed in those regions. We therefore propose that *ZmTML1* acts downstream of mechanisms that
311 spatially regulate where veins are initiated, acts earlier than *ZmHB52* in vein development, and that
312 any role in specifying procambial initial cells is carried out redundantly with other (as yet unidentified)
313 partners such that procambium is positioned in the correct locations in mutant leaves.
314
315 Of the 529 differentially expressed transcription factor (TF) encoding genes (L2FC > 1; $p < 0.05$),
316 greater than 4-fold differences in transcript levels between wild-type and mutant were observed for
317 members of 24 different TF families (**Figure S4C**). Twenty-fold higher levels of *ZmGRF1* (*GROWTH*
318 *REGULATING FACTOR 1*) transcripts in mutants than in wild-type segregants were particularly
319 notable because *ZmGRF1* transcript levels are normally tightly regulated post-transcriptionally by
320 miR396a [44]. Whatsmore, constitutive overexpression of a miRNA-resistant version of *ZmGRF1* in
321 maize was associated with a larger cell division zone at the base of developing leaves, with increased
322 numbers of normal sized cells dividing more slowly than in wild-type counterparts [45]. Upregulation of
323 *ZmANT1* (*ZmEREB184*) (L2FC > 6; $p < 0.05$) in mutants (**Figure S4C**) is also notable in this regard
324 because of a proposed role in cell proliferation during leaf development [46]. As such, the phenotype of
325 *Zmtml1tml2* mutant leaves may be caused in part by altered cell division dynamics in developing leaf
326 primordia and *ZmGRF1* and/or *ZmANT1* expression may be directly or indirectly repressed by ZmTML1
327 and/or ZmTML2.
328
329 Because the spatial and temporal extent of cell division zones within developing grass leaves has been
330 associated with the regulation of cytokinin signalling (CK) (higher levels are present in the division
331 zone) [47,48], and GO-terms associated with CK were enriched in the population of differentially
332 expressed genes (**Figure 4A**), we next sought to determine which components of the cytokinin pathway
333 were perturbed in *Zmtml1tml2* mutants. To this end, we compiled a list of genes involved in cytokinin
334 biosynthesis, signalling, degradation and response (**Supplementary File 10**), and quantified transcript
335 levels for each in mutant and wild-type tissues. Of the 150 genes analysed, 11 exhibited significant
336 differences between wild-type and mutant (**Supplementary File 10**, **Figure 4B**). The most substantial

differences were seen for transcripts encoding two histidine kinase CK receptors (decreased in the mutant by more than 9-fold (*ZmHK1/HSF1* [49]) and 7-fold (*ZmHK5*)), a homolog of the CK efflux transporter ABCG14 in Arabidopsis [50] (reduced more than 7-fold in the mutant) and the cytokinin oxidase degrading enzyme ZmCKX11 [51] (increased more than 4-fold in the mutant). Collectively these observations suggest that overall CK activity is repressed in *Zmtml1tml2* mutant apices and thus that cell division dynamics may be perturbed in the shoot apical meristem and/or leaf primordia.

Given that a role for auxin in leaf venation patterning is well established, we predicted that components of the auxin pathway would also be perturbed in *Zmtml1tml2* mutants. Indeed, significant differences were observed in levels of transcripts encoding a number of AUXIN RESPONSE FACTORs (ARFs) that bind directly to the promoters of auxin responsive genes (reviewed in [52]) (**Figure S4C**). To determine the point(s) at which perturbations in the auxin pathway were manifest, we compiled a list of genes involved in auxin biosynthesis, conjugation, transport, signalling and response and quantified transcript levels for each gene (**Supplementary File 11**). Of the 186 genes analysed, 31 exhibited significant differences between mutant and wild type (**Figure 4B, Supplementary File 11)**. Although all steps of the pathway showed some perturbation, biosynthesis and transport steps were least impacted suggesting that these are upstream of TML function. With the exception of *ALDEHYDE OXIDASE1* (*ZmAO1*), where transcript levels were elevated over 20-fold in the mutant, the most substantial differences in transcript levels were seen for genes encoding components involved in auxin signalling. Aldehyde oxidases have been implicated in the synthesis of tryptophan precursors for IAA biosynthesis [53]. However, direct functional analyses are lacking and given that there is no evidence that downstream components of the auxin biosynthesis pathway are similarly elevated we cannot speculate on the significance of any potential increase in tryptophan levels. Of the signalling components: *ZmSAR1*, *ZmARF4* and *ZmARF3* were downregulated more than 7-fold in the mutants; *ZmARF39/ZmABI17*, *ZmARF36* and *ZmARF13* were upregulated more than 7-fold in the mutant; and *ZmARF30* and *ZmARF16* were upregulated more than 4-fold in the mutant. Note that *ZmARF4* is a co-ortholog (with *ZmARF29*) of *MP* in Arabidopsis, mutations in which reduce the complexity of leaf venation patterns and disrupt axis formation in the embryo [54,55]. *ZmSAR1* encodes the ortholog of Arabidopsis SUPPRESSOR OF AUXIN RESISTANCE 1, which is a nucleoporin that facilitates nuclear localization of AUX/IAA proteins [56]. Reduced *ZmSAR1* transcript levels may thus suggest that the ability of AUX/IAA proteins to bind and repress ARFs is compromised in *Zmtml1tml2* mutants, which would translate into increased activation of ARF proteins. Notably, the three most highly upregulated *ARF* genes in *Zmtml1tml2* mutants are class B repressors and the two downregulated *ARF* genes are class A activators [57]. The loss of ZmTML function may thus lead to an overall repression of auxin responses, but the possibility that responses are differentially up- or down-regulated in different spatial domains of the shoot apex cannot be discounted.

376 **Transgenic lines that constitutively express *ZmTML1* in rice could not be isolated**

377 With the finding that *ZmTML1* represses lateral vein formation, we hypothesized that ectopic
378 expression in rice would increase the number of intermediate veins in the leaf. Given that a higher
379 proportion of intermediate veins is a key trait of C_4 leaves, and an engineering goal is to make rice
380 leaves more C_4-like [58,59], we first tried to constitutively express *ZmTML1* in rice. Constructs in which
381 expression of the maize *TML1* coding region was driven by the constitutive maize ubiquitin promoter
382 (**Figure S5A**) were transformed on multiple occasions (n=7) and callus was propagated to the greening
383 stage on selection medium, however, shoots could not be regenerated. This observation suggested
384 that *ZmTML1* may suppress the formation of all veins and/or the pluripotency required for shoot
385 regeneration.

386

387 ***TML* promoter activity is suppressed in transgenic rice lines**

388 The failure to regenerate rice callus that constitutively expressed the *ZmTML1* gene from maize led us
389 to consider that gene dosage and/or expression levels may need to be tightly regulated (spatially and/or
390 temporally). To generate a chassis in which we could test this hypothesis, we therefore edited the
391 endogenous rice gene. The rice genome contains a single *OsTML* (*OsWIP6*) gene
392 (LOC_Os09g13680) which encodes a protein with 71.4 % amino acid identity to the maize protein.
393 Edited alleles were generated either using a single guide RNA sequence (sgRNA1) that was designed
394 to target between the EAR and zinc finger domains or by using sgRNA1 along with two additional
395 guides (sgRNA3 and sgRNA4) that targeted the 5' and 3' regions of the coding sequence, respectively
396 (**Figure 5A**). A total of five loss of function alleles were isolated from the two independent
397 transformation experiments. The mutant alleles contained short indels at single or multiple guide sites
398 that shifted the reading frame to result in aberrant or truncated proteins (**Figure 5B**). All edited T0
399 plants were either homozygous for the mutation or heteroallelic. After backcrossing to WT,
400 heterozygous F1 plants were self-pollinated and F2 populations segregated mutant progeny as a
401 recessive trait. Notably, all plants carrying loss of function alleles showed an increased proportion of
402 larger, lateral-like veins in the leaf blade (**Figure 5C**) suggesting that *TML* gene function is conserved
403 in maize and rice.

404

405 The similar phenotypes of *Zmtml1* and *Ostml* mutants suggest that any TML-mediated difference in
406 venation patterns between the two species must result from different domains of activity in the leaf. We
407 thus revisited the question of whether maize-type expression patterns could alter venation patterns in
408 rice and transformed the *ZmTML1* gene under the control of its own promoter (**Figure S5B, File S12**)
409 into the *Ostml* mutant and wild-type Kitaake rice. Five hygromycin resistant transgenic lines were
410 obtained in the *Ostml_m1* background and 24 lines in the wild-type background but no phenotypic
411 changes were detected in any of the lines tested. This observation suggested either that the *ZmTML1*
412 gene had recombined out of the transgene construct, that the *ZmTML1* promoter sequence did not
413 contain essential regulatory regions, or that transgene expression was suppressed.

414

415 Given that we were unable to obtain transgenic lines that expressed *ZmTML* from either a constitutive
416 promoter or from its own promoter, we tested whether endogenous *OsTML* expression patterns could
417 be faithfully reproduced in a series of complementation experiments. First, a 2945 bp promoter
418 sequence located directly upstream of the start codon and containing a regulatory region predicted by
419 ATAC sequencing was fused to the *OsTML* coding sequence and to either the *nos* terminator (construct
420 1), the *nos* terminator plus 458 bp of the *OsTML* 3'UTR that contained an 83 bp element conserved in
421 rice, maize and setaria (construct 2) or ~1 kb of *OsTML* sequence downstream of the stop codon
422 (construct 3) **(Figure 5D)**. The three constructs were individually transformed into wild-type and
423 *Ostml_m1* (construct 1) or *Ostml_m2* and *Ostml_m3.1* (constructs 2 & 3) lines. In each case transgenic
424 plants were successfully regenerated on selection medium but no complementation was observed (see
425 examples in **Figure S5C, D**). As with *ZmTML1*, therefore, the transgenic rice promoter sequence was
426 either lacking essential elements or expression was suppressed. To distinguish between these two
427 possibilities, two further constructs were tested (**Figure 5D**). One contained the *OsTML* genomic region
428 comprised of 5.35 kb of upstream sequence, both exons and the intron, plus 458 bp of downstream
429 sequence (construct 4). Because the upstream genomic region contained multiple transposon
430 sequences which may induce host silencing responses, these were removed in the second construct,
431 leaving the ATAC sequence fused directly to the proximal promoter (construct 5). Both constructs were
432 transformed into the *Ostml_m3.1* background but neither complemented the mutant phenotype (**Figure**
433 **S5C, D**). Although still formally possible that essential elements were missing from the genomic
434 constructs, this observation suggested that transgene expression was being suppressed, even in the
435 absence of transposon sequences within the promoter. To test this hypothesis, seed from lines
436 containing construct 2 were germinated on 50 mg/L 5-azacytidine to demethylate the genome.
437 Although pleiotropic, this treatment lead to complementation of the *Ostml* mutant phenotype,
438 presumably by activating *OsTML* transgene expression (**Figure 5E**). Collectively these observations
439 suggest that *TML* gene expression is tightly regulated *in planta* and that any mis-expression (spatial
440 and/or temporal) induced via transgenesis is likely to be suppressed or to cause developmental arrest.
441

442 **Loss of function mutations in *OsTML* specifically alter venation patterns in the leaf**

443 Given the inability to modify *TML* expression patterns in rice, we characterized loss of function *Ostml*
444 mutants in detail to determine the extent to which venation patterns are perturbed. Three independent
445 lines were backcrossed to the wild type and selfed prior to examining overall growth phenotypes. In
446 terms of overall morphology the mutant lines did not differ substantially from null segregants (**Figure**
447 **6A**) although *Ostml-m3.1* plants were shorter than wild-type (**Figure S6A**). All mutant lines showed a
448 significantly increased number of lateral veins in the leaf blade (**Figure 6B, 6C**), a decreased number
449 of intermediate veins (**Figure 6D**) but no significant change in vein density (**Figure 6E**). There were no
450 apparent vascular defects in the roots, rachis or pedicel of mutant plants (**Figure S6B-D**) but venation
451 defects in the leaf were apparent as early as P3, where veins developing in the position of intermediate
452 veins were visibly larger in mutants than in corresponding wild types (**Figure S6E, F**). Importantly, the
453 alterations to vein patterning were accompanied by altered bundle sheath cell occupancy in the leaf.

454 In wild-type rice, bundle sheath cells are rectangular when viewed paradermally, with the long edges
455 running parallel to the associated vein and the short edges aligned with the medio-lateral leaf axis
456 (**Figure 6F**). The length of individual bundle sheath cells around veins is highly variable but
457 quantification revealed no significant differences between the length of cells around lateral versus
458 intermediate veins in wild-type, *Ostml_m3.1* and *Ostml_m3.3* mutant samples (**Figure 6G**). The one
459 exception to this was seen in *Ostml_m4* mutants where cells around both lateral and intermediate veins
460 were significantly shorter than those in wild-type (**Figure 6G**). As a consquence of the increased
461 proportion of lateral veins in mutant leaves, when viewed transversely, total bundle sheath cell number
462 across the medio-lateral leaf axis is higher in all mutants as compared to wild-type (**Figure 6B, 6H**).
463 When the altered cell number across the medio-lateral axis is adjusted to account for any variations in
464 cell length along the proximo-distal axis, mutant leaves are seen to have an increase in bundle sheath
465 cell number of 9-23% per unit area as compared to wild type (**Figure 6H**). Collectively these
466 observations suggest that although there are no alterations in vein density in the *Ostml* mutant leaves,
467 vein occupancy in the leaf is increased and there is a substantial increase in the number of bundle
468 sheath cells.
469
470 **DISCUSSION**
471 Through loss of function analyses in three monocot species we have identified a conserved role for
472 WIP6 orthologs in the specification of vein rank in developing grass leaf primordia **(Figures 3, 5, 6 &**
473 **S3)**. WIP6 orthologs have been identified in the genomes of all vascular plant groups, as have
474 members of the sister WIP1-5 clade, but just a single *WIP* gene is present in the non-vascular
475 bryophyte *Marchantia polymorpha* [60] (**Figure 1**). The finding that the *MpWIP* gene is required for the
476 development of air pore complexes on the dorsal surface of the thallus led to the suggestion that prior
477 to a gene duplication in the last common ancestor of lycophytes and euphyllophytes (ferns,
478 gymnosperms and angiosperms), WIP gene function was required for the differentiation of multicellular
479 structures [60]. This suggestion is consistent with the observation that members of the WIP1-5 clade in
480 Arabidopsis have been shown to play a role in the development of transmitting tract tissue in the pistil
481 (WIP2) [61], the seed coat (WIP1) [31], and the root (WIP2/4/5) [62], specifically in the regulation of cell
482 division orientation in stem cells and cell-type specification. However, a role for WIP6 has not been
483 unambiguously defined in Arabidopsis. Original reports of leaf venation defects in loss of function
484 mutants [32] were later invalidated [34] and the suggestion of a non cell-autonomous role in maternal tissue
485 to suppress cell-type specification in embryonic roots was only inferred from the phenotype of
486 combined triple *wip1/3/6* mutants [33]. To our knowledge, there are no reports of phenotypic perturbations
487 in single *wip6* loss of function mutants in any eudicot.
488
489 On the basis of the conserved phenotype observed in loss of function *wip6* mutants in maize, *S. viridis*
490 and rice, we named WIP6 orthologs *TOO MANY LATERALS* (*TML*). The spatial expression of *TML*
491 genes in procambial initial cells, the temporal restriction of expression to the first few divisions of those
492 cells and the mis-specification of intermediate veins as laterals in mutant leaves (**Figures 2, 3, 5, 6,**

493 **S2, S3 & S4**) are all consistent with a role in cell-type specification and/or divisions of procambial cells
494 in the leaf. The mutant phenotype is also consistent with the role inferred from triple *wip1/3/6* mutants
495 in Arabidopsis, namely that of a suppressor [33]. A repressor role is further supported by the observation
496 that constitutive expression of *AtWIP6* conditions a small leaf phenotype in Arabidopsis [63]. Notably,
497 general repression of organ growth by WIP proteins has also been demonstrated in other species. For
498 example, in melon the WIP1 ortholog *CmWIP1* regulates sex determination by repressing carpel
499 primordia in male flowers [64] and overexpression of the WIP2 ortholog in *Gerbera hybrida* suppresses
500 growth in multiple organs [65]. This general repressive role likely explains the failure to regenerate rice
501 callus after transformation with a construct that constitutively expressed *ZmTML1* (**Figure S5**). It may
502 also explain why attempts to express *TML* genes in rice from the corresponding maize or rice promoters
503 led to transgene silencing **(Figure 5)**. Possibly, the repressive function of TML is only tolerated in the
504 first few divisions of procambial cells in leaf primordia and as such any leaky expression in callus is
505 silenced. Considering all of these factors, we propose that TML functions in grasses to suppress cell
506 divisions and/or cell fate decisions in procambial cells that normally lead to the formation of lateral
507 veins, consequently enabling intermediate veins to develop.
508
509 The role of TML as a suppressor of lateral vein formation as opposed to an activator of intermediate
510 vein formation is intriguing, not least because it only functions in a subset of the rank 1 intermediate
511 veins. All intermediate veins differentiate from the tip of the leaf primordium towards the base, but only
512 the largest and first to initiate extend into the leaf sheath [17,18]. It is these large intermediate veins that
513 are converted to laterals in *tml* mutants of both maize and rice. The rank 1 intermediate veins that only
514 differentate sclerenchyma on the abaxial or adaxial side and the rank 2 intemediate veins that only
515 develop in C_4 leaves are unaffected in mutant leaves **(Figures 3, 5 & 6)**. This phenotypic distinction in
516 mutants is reflected in the spatial distribution of *TML* transcripts during wild-type development **(Figures**
517 **2 & S4)** and thus regulators that activate *TML* transcription and or transcript stability determine which
518 procambial cells are subject to TML-mediated suppression. To date only one transcription factor that
519 binds *in vitro* to the *ZmTML1* promoter has been identified [66] and no function has been assigned to
520 *ZmbHLH105* or any of its orthologs. Although direct activators of TML activity are unknown, at some
521 level the PIN1/auxin traces that precede the formation of all vein ranks [24] must be interpreted differently
522 in procambial initial cells that develop the different vein-types, leading to TML activity in some but not
523 all of those cells.
524
525 Transcriptome comparisons between wild-type and mutant shoot apices in maize have provided some
526 insight into perturbations caused by loss of TML function, however, because *TML* is expressed in just
527 a few cells and only for a short time, the likelihood of identifying direct targets in this dataset is low.
528 Observed perturbations in both auxin and cytokinin pathways **(Figures 4 & 4S)** could be a direct
529 consequence of loss of TML function but there is insufficient spatial resolution in whole tissue
530 transcriptomes to validate this suggestion. Specifically, the apparent suppression of both pathways
531 observed in whole shoot apices could be masking significant increases in activity that are spatially or

532 temporally localized. Mechanistically, the presence of an EAR domain [38] in the TML protein is of note
533 because EAR domains bind TOPLESS proteins, which themselves recruit epigenetic modifiers [37]. It is
534 therefore possible that promoters bound by the zinc finger domain of TML are silenced. In this regard,
535 a 20-fold increase in levels of transcripts encoding the growth regulating factor *ZmGRF1* in *Zmtml1tml2*
536 mutant leaves is notable. Although direct targets have yet to be identified, we propose that TML either
537 represses a target gene that positively regulates lateral vein identity or that TML-mediated regulation
538 of cell divisions in procambial initial cells prevents specific division orientations that are required for
539 lateral vein formation.
540
541 Unlike in eudicots, where venation patterning in the leaf has been perturbed by mutations in a number
542 of genes that are not directly associated with auxin signaling (e.g. *cotyledon vascular pattern* [67] and
543 *thickvein* [68]) most venation defects in grass leaves reported to date have resulted from indirect
544 perturbations to hormone pathways, mis-specification of blade versus sheath domains, and/or the
545 regulation of leaf width. For example, growth of maize on auxin transport inhibitors converted blade
546 tissue into sheath, with a consequent alteration in vein spacing across the medio-lateral leaf axis [69]. A
547 similar blade to sheath transition was observed in sorghum mutants defective in a cytochrome P450
548 required for brassinosteroid biosynthesis [70] and in gain of function rice mutants that lead to an up-
549 regulation in cytokinin signaling [71]. In rice, mutants with higher vein density invariably had narrower
550 leaves and smaller mesophyll cells between veins [72,73] and in the case of the *narrow leaf 1* mutation,
551 that defect was associated with reduced polar auxin transport [74]. The only mutation reported to directly
552 perturb procambium formation in rice leaves (*radicleless1*), also failed to form an embryonic root [75].
553 Notably, this pleiotropic phenotype is also observed in the Arabidopsis auxin response mutant
554 *monopteros* but *MP* is known to play a direct role in the leaf vein formation [55]. In contrast to all of these
555 examples, the role of *TML* in vein development is confined to the leaf, providing an opportunity to
556 manipulate vein patterning in rice for future metabolic engineering of C_4 photosynthesis. An optimal
557 chassis for C_4 engineering would have normal leaf width, vein pairs separated by just two mesophyll
558 cells and a 1:1 ratio of bundle sheath to mesophyll cells. Loss of TML function does not achieve that
559 goal, however, mutant leaves have a significant increase in the overall volume of leaf veins and in the
560 number of bundle sheath cells. The leaf-specific defects in *Ostml* mutants thus represent a fundamental
561 advance in our understanding of how veins are patterned in grass leaves and provide the first step
562 towards engineering the anatomy required to underpin C_4 photosynthesis.
563

564 **METHODS**

565 *Phylogenetic analysis*

566 For the WIP family tree, the complete set of predicted proteomes for all species in Phytozome version
567 12 [76] were subject to orthogroup inference using OrthoFinder [30]. The orthogroup containing the maize
568 gene GRMZM2G150011(v3 genome)/ Zm00001d020037(v4 genome)/Zm00001eb309530 (v5
569 genome) was identified and the 379 constituent protein sequences (**Supplementary File 1**) subject to
570 multiple sequence alignment using MergeAlign [77]. The alignment was then imported into MEGA [78] and

571 trimmed to contain the EAR domain plus the zinc finger region. After empirical testing of the multiple
572 sequence alignment for maximum likelihood phylogenetic tree inference using IQTREE [79], 11
573 sequences that failed the composition χ^2 test and 21 sequences that had more than 50% gaps were
574 removed. After realignment of the remaining 347 sequences using MergeAlign (**Supplementary File**
575 **2**), the best-fitting model parameters (JTT+I+G4) were estimated and a consensus phylogenetic tree
576 was estimated from 1000 bootstrap replicates (**Supplementary File 3**). The data were imported into
577 ITOL [80] to generate the pictorial representation. Branches with less than 50% bootstrap support were
578 deleted and three leaves that were incorrectly positioned in the WIP2/4/5 clade (likely due to mis-
579 annotation of the corresponding sequences) were deleted (Asparagus v1 05.3078 – positioned in a
580 eudicot clade, *H. annus* chr02g0056311 – positioned in a monocot clade, and *Zostera marina*
581 Zosma112g00240.1 – splitting gymnosperm and Amborella).
582
583 For the WIP6 tree, sequences were selected from two bryophytes (to root the tree), 6 eudicots and 7
584 monocots (**Supplementary File 4**). Species were chosen primarily to resolve relationships within the
585 Panicoid grasses but also to represent the major flowering plant groups (monocots, asterids and
586 rosids). Sequences were retrieved by BLAST searches of Phytozome 13 and NCBI and aligned with
587 MAFFT using the L-INS-i refinement method [81] (**Supplementary File 5, Supplementary Figure 1A**).
588 IQTree [79] was used to estimate the best-fitting model parameters (JTT+F+I+G4) and to infer a
589 consensus phylogenetic tree from 1000 bootstrap replicates (**Supplementary File 6**). The data were
590 imported into ITOL to generate the pictorial representation. Notably it was extremely difficult to align
591 sequences between the EAR and WIP domains across a broad phylogenetic range, with blocks of
592 sequence conserved within groups (e.g. grasses and brassicas) but highly variant between groups
593 (**Supplementary Figure 1B, Supplementary File 7**). Despite a high level of sequence conservation
594 across the zinc finger domains, this variability constrained the number and identity of eudicot species
595 for which tree inference was supported with high bootstrap values.
596
597 *Plant material and growth conditions*
598 Maize (inbreds B73 and B104) and *Setaria viridis* (accession ME034V) seeds were germinated as
599 previously described [41,43]. Both species were grown in a greenhouse with a long day (16 h light / 8 h
600 dark) photoperiod with 28 °C day / 20 °C night temperatures. Under low natural light conditions (below
601 120 µmol photon m^{-2} s^{-1}) plants were provided with supplemental light. Rice (*spp japonica cv* Kitaake)
602 seeds were sterilized and germinated in petri dishes containing ½ MS medium under a 16 h light /8 h
603 dark photoperiod, 30 °C day/ 25 °C night temperatures. Seven days after plating, seedlings were
604 transferred to falcon tubes containing ¼ MS medium. Two-week-old seedlings were transferred to clay
605 pots and grown under the same conditions described above.
606
607 *In situ hybridization*
608 *In situ* hybridization was carried out using wax-embedded shoot apices as described by Schuler et al.
609 [82], with digoxygenin (DIG)-labelled RNA probes designed to specifically detect *ZmWIP6A, ZmWIP6B,*

610 *OsWIP6, SbWIP6* or *SvWIP6* transcripts. The *ZmWIP6A* probe was a 427 bp fragment spanning 141
611 bp of the 5'UTR and the first 286 bp of the coding sequence. The probe shared 53% similarity with the
612 corresponding region of the *ZmWIP6B* transcript sequence. The *ZmWIP6B* probe was a 203 bp
613 fragment encompassing the end of the coding sequence and part of the 3'UTR. The probe shared 52%
614 similarity with the corresponding region of the *ZmWIP6A* transcript sequence. The *OsWIP6* (142 bp),
615 *SbWIP6* (393 bp) and *SvWIP6* (214 bp) probes encompassed the beginning of the first exon and
616 included the EAR domain. Post-hybridization washes were undertaken with 0.005 x SSC buffer made
617 from a 20x SSC stock (3M NaCl, 0.3M Na_3citrate), calculated to ensure stringency.
618
619 *Molecular Cartography probe design*
620 Probes were designed using Resolve BioSciences' proprietary design algorithm and gene annotations
621 from the Zea Mays RefGen V4. The final set of probes was selected with the methodology described
622 in Glenn et al. [83].
623
624 *Tissue preparation and Molecular Cartography hybridization*
625 Wild-type B73 seeds were germinated and grown in an environment-controlled chamber on a 16 h/8 h
626 day/night cycle, temperature 28 °C/20 °C, 50 % humidity and light intensity of 300 µmol m^{-2} s^{-1}. Seeds
627 were germinated in medium vermiculite and seedlings were harvested ten days after sowing. Maize
628 shoot apices were cut just below and 0.5 cm above the shoot apical meristem and immediately fixed
629 in 4 % paraformaldehyde, dehydrated, and embedded in Paraplast Plus following the user guide for
630 sample preparation from Resolve BioSciences. Clearing and wax infiltration were either carried out
631 manually or in a TissueTek VIP processor. Wax-infiltrated samples were embedded in blocks of
632 Paraplast Plus using a TissueTek TEC wax-embedding centre. A total of six 10 µm transverse sections
633 across two experiments were cut with a microtome and baked onto a Molecular Cartography-
634 compatible coverslip at 37 °C overnight to allow for sample attachment. Sections were then
635 deparaffinized, permeabilized, and refixed according to the user guide. After complete dehydration, the
636 sections were mounted using SlowFade-Diamond Antifade mounting medium, covered with a glass
637 coverslip and shipped to Resolve BioSciences for analysis.
638
639 At Resolve BioSciences, sections were washed twice in phosphate buffered saline for 2 min, followed
640 by 1 min washing in 50% and 70% ethanol at room temperature. Ethanol was removed by aspiration
641 and DST1 buffer was added, followed by tissue priming for 30 min at 37 °C and by a 48 h hybridization
642 using probes specific for the target genes. Samples were washed to remove excess probes and
643 fluorescently tagged in a two-step color development process. Fluorescent signals were removed after
644 imaging in a decolorization step. Colorization, imaging, and decolorization were iterated for multiple
645 cycles to generate a unique combinatorial code for each target gene. Samples were imaged by Resolve
646 BioSciences as described in Glenn *et al.* [83].
647
648

649 *Pre-processing of Molecular Cartography images and cell segmentation*
650 Cell segmentation was carried out using CellPose 2.0 [84], starting from high resolution images of
651 Calcofluor and DAPI-stained sections. A pre-processing step was carried out to facilitate cell
652 segmentation. Firstly, DAPI and Calcofluor images were overlaid in ImageJ: the co-existence of cell
653 wall and nuclear staining allows for more accurate segmentation with CellPose. Subsequently, different
654 stages of leaf development were cropped and isolated from the overlay image: this allows for faster
655 computational speed during the segmentation step, and for a more accurate estimate of the average
656 cell diameter, which varies greatly between leaf primordia. The images of isolated leaf primordia were
657 imported into CellPose, and the Calcofluor and DAPI channels brightness and contrast were adjusted
658 as required. The "cyto2" model was used to predict the cell boundaries in meristem/P1 and P2
659 primordia, whereas the "TN2" model was used to predict cell boundaries in P3, P4 and P5 primordia.
660 All segmentations were then manually corrected, and the resulting masks were used to train a custom
661 model. All subsequent primordia underwent segmentation using the custom models thus obtained and
662 corrected manually where required. Segmented cells were exported as PNG masks and converted to
663 ROIs using the ImageJ plugin "Labels to ROIs". ROIs were then used to visualize single-cell gene
664 expression using the proprietary Molecular Cartography plugin from Resolve Biosciences.
665
666 *CRISPR construct design*
667 Short RNA guides targeting *ZmWIP6A, ZmWIP6B, SvWIP6 and OsWIP6* were designed using the
668 online guide RNA selection tool, CRISPOR [85]. For maize and setaria, two guide RNAs were designed
669 to target each *WIP6* gene within the first exon. In the case of *OsWIP6* three guides were used, sgRNA1
670 and sgRNA3 in the first exon and sgRNA4 in the 3'UTR to potentially generate large deletions in
671 combination with the first two guides.
672
673 The four maize guides targeting *ZmWIP6A* (sgRNA25: TGGTACGAGTGATGAGTGTA & sgRNA194:
674 CGCAGCCGGCATTATTGTAA) and *ZmWIP6B* (sgRNA28: TGCTGGTACGGGTGAGCGTA &
675 sgRNA309: CAGATCCGCCGCCATTGTAA) were cloned in vector pMHb-pZmUBIL-ZmCas9-NosT-
676 AG-pBdEF1a-tdTomato-NLS-NosT (https://gatewayvectors.vib.be/).
677
678 The rice and setaria sgRNAs were cloned downstream of the OsU3 promoter in the Golden Gate
679 system [86] as previously described [42]. The setaria guides sgRNA77: CTCATCCTACTCGGCATGCT and
680 sgRNA153: CCGTTCCCCCCAGCAACAAG were assembled in construct EC17847. The rice guides
681 were used to generate two separate constructs, EC17627 containing only sgRNA1:
682 TTCAACCCGAGCCACTACCA and EC17697 containing sgRNA1, sgRNA3:
683 CACCTGTACCAGAGCCACCA and sgRNA4: CGTACAGTCTAGCTAGGTAT. The Cas9p gene [87] was
684 expressed under the control of the *ZmUbi* promoter and the selection module contained a hygromycin
685 resistance gene driven by the *OsAct1* promoter.
686
687

688 *Overexpression and complementation construct design*

689 The *ZmUbi*$_{pro}$: *ZmTML1* overexpression construct was obtained by cloning the *ZmTML1* ORF into the
690 binary destination vector pVec8-Gateway [88]. The *ZmTML1* ORF was amplified by polymerase chain
691 reaction (PCR) using maize B73 genomic DNA as template and Gateway® compatible primers (MS.
692 F: 5'-TCAGCAGACCACCACCCAAT-3'; MS. R: 5'-CTAGATGACGACCATGTCGCTGG-3'). The PCR
693 product was cloned into Gateway® donor vector pDONR™207, sequenced, and subsequently cloned
694 downstream of the *ZmUBI* promoter in the binary destination vector pVec8-Gateway.
695
696 *OsTML* complementation constructs 1, 2 and 3 were cloned into the Golden Gate system which
697 required BpiI or BsaI enzyme recognition sites to be domesticated. The *OsTML* cDNA sequence was
698 obtained by synthesis with one BpiI site 'domesticated'. The 2945 bp promoter region, *OsTML*
699 terminator region and the 3' UTR were cloned from PCR amplified fragments. As the *OsTML* promoter
700 contained two BsaI and one BpiI enzyme recognition sites, primers were designed both to 'domesticate'
701 the restriction sites (by introducing three single bp changes) and to generate BpiI sites at the ends.
702 This allowed promoter assembly using a Golden Gate cloning strategy and without introducing any
703 other scars in the sequence. The *OsTML* terminator region and 3'UTR did not require domestication.
704
705 To avoid any modification that could potentially alter promoter function, the fourth version of the
706 complementation construct was assembled using NEBuilder HiFi DNA Assembly strategy. A ~7 kb
707 genomic region was amplified by PCR in four overlapping fragments. The fragments were assembled
708 into a Golden Gate level 2 vector containing the hygromycin selection module. To obtain the 'ATAC'
709 version (construct 5), the construct above was cut with PmeI/FspI to remove most of the promoter
710 sequence apart from 545 bp adjacent to the ATG. A PCR amplified 540 bp fragment overlapping the
711 predicted 'ATAC' region was then added in a NEBuilder HiFi DNA Assembly reaction. The ATAC
712 sequence information for both maize [89] and rice [90] was accessed via the Plant Epigenome Browser -
713 https://epigenome.genetics.uga.edu/PlantEpigenome/index.html. Primer sequences for Golden Gate
714 and NEBuilder HiFi DNA Assembly are listed in **Supplementary Table 1.**
715
716 *Plant transformation*

717 Maize CRISPR lines were generated in inbred line B104 at the VIB Ghent Crop Genome Engineering
718 Facility (https://www.psb.ugent.be/cores/crop_genome_engineering_facility). Backcrossed T1 seeds
719 were provided for 10 independent lines.
720
721 Transgenic rice (*O. sativa ssp. japonica* cv. Kitaake) lines were obtained following a modified callus
722 transformation protocol from Toki et al. [91]. The modified protocol is available at
723 https://langdalelab.files.wordpress.com/2015/07/kitaake_transformation_2015.pdf.
724
725 To generate setaria CRISPR edited lines, construct EC17847 was transformed into accession ME034V
726 following a protocol described by Hughes *et al.* [43].

727 Regenerated rice and setaria T0 plantlets were verified by PCR with primers targeting the selection
728 gene hygromycin phosphotransferase (hpt) (forward primer: 5'- CAACCAAGCTCTGATAGAGT- 3';
729 reverse primer: 5'- GAAGAATCTCGTGCTTTCA-3') to confirm successful transgene insertion in the
730 genome. Plants genotyped positive for hpt were potted in clay and watered with fertilizer solution in a
731 semi-hydroponic setting.
732
733 *Phenotyping leaf anatomy*
734 Leaf segments (3-4mm) spanning the whole leaf width were collected from the widest part of fully
735 expanded leaves, which in maize and setaria localized to the middle of the blade and in rice to the
736 upper third of the blade. Leaf seven was analysed in rice, and leaf five in maize and setaria. The
737 samples were fixed in 3:1 ethanol: acetic acid for 30 min at room temperature and transferred to 70 %
738 ethanol. Fixed samples were placed into tissue embedding cassettes, dehydrated and infiltrated with
739 Paraplast Plus in a Tissue Tek Vacuum Infiltration Processor. Wax infiltrated samples were set in
740 blocks, trimmed and sectioned using a Leica RM2135 rotary microtome. 10 µm transverse sections
741 were placed onto microscope slides and dried at 37 ^{o}C overnight before dewaxing and staining. For
742 paradermal sections, fragments of rice leaf blade without the midvein were flattened and stacked using
743 0.8 % agarose layers before wax embedding and sectioning as described above.
744
745 Leaf sections were treated with histoclear to remove wax, partially rehydrated in 70 % EtOH prior to
746 staining for 30 min with Safranin O (1 % in 50 % EtOH). The slides were then stained for 30 sec with
747 Fast Green FCF (0.03 % in 95 % EtOH), dehydrated, drained and mounted using DPX.
748
749 Sections were viewed and imaged with a Leica DMRB microscope. Images were used to estimate leaf
750 width, vein density and quantification of each vein type (lateral, rank1 intermediates and rank 2
751 intermediates). Paradermal sections were imaged to allow bundle sheath cell length to be measured.
752
753 *RNA sequencing, transcript quantification and differential expression*
754 Maize shoot apices were dissected from vermiculite-germinated 7-day-old *Zmtml1tml2* seedlings and
755 genotypically segregating wild-type siblings. Total RNA was extracted from three individual shoot
756 apices using the Qiagen RNeasy Plant Mini Kit (Cat. No. 74904). Subsequent DNase treatment was
757 done using the Ambion® TURBO DNA-free™ Kit (Cat. No. AM1907). RNA quantity was checked and
758 normalized using a Qubit™ RNA HS Assay Kit. RNA quality was assessed with an Agilent RNA 6000
759 Nano Kit ensuring that all RNA used for library preparation had a RIN value ≥ 9.0. Strand-specific RNA
760 sequencing library preparation and sequencing was conducted by the Oxford Genomics Centre at the
761 Wellcome Centre for Human Genetics (funded by Wellcome Trust grant reference 203141/A/16/Z).
762 Sequencing was performed on an Illumina NovSeq6000 with paired-end 150-bp reads. Sequenced
763 reads were mapped to the Zea Mays B73 RefGen V4 genome (https://phytozome-
764 next.jgi.doe.gov/info/Zmays_RefGen_V4) using STAR [92], transcript quantification was done with
765 Salmon [93] and differential gene expression was determined using DESEq2 [94]. The identification of

766 differentially expressed genes was based on having log 2-fold change (L2FC) ±1, with an adjusted p-
767 value <0.05.
768
769 *Differential expression data sub-setting and enrichment analysis*
770 A subset of genes that were differentially expressed between *Zmtml1tml2* plants and genotypically
771 segregating wild-type siblings were classified as transcription factors using the Grassius Maize
772 Transcription Factor Database (https://grassius.org/browsefamily/Maize/TF) annotations. Lists of B73
773 RefGen V4 IDs of genes belonging to each specific transcription factor family were downloaded and
774 cross-referenced with the differentially expressed gene list using R scripts (available upon request).
775 Genes known to have a role in auxin and cytokinin pathways were compiled and curated from searches
776 of both the literature [95] and databases (AmiGo knowledgebase [96], PANTHER [97] and UniProt [98]) using
777 the search words "auxin" or "cytokinin".
778
779 *Enrichment analysis*
780 Statistical overrepresentation test (ORA) of Gene Ontology annotation set "GO biological process
781 complete" was performed using the PANTHER 17.0 GO Ontology database version (DOI:
782 10.5281/zenodo.7942786 Released 2023-05-10) with a Fisher's Exact test type and a false discovery
783 rate correction. The reference list comprised of all significantly differentially expressed genes between
784 the *Zmtml1tml2* plants and genotypically segregating wild-type siblings. The significantly up-regulated
785 (L2FC > 1; padj <0.05) and significantly down-regulated (L2FC < 1; padj <0.05) datasets were tested
786 separately. A subset of the differentially expressed genes between *Zmtml1tml2* plants and
787 genotypically segregating wild-type siblings were classified as transcription factors using the Grassius
788 Maize Transcription Factor Database [99] annotations. An independent ORA was conducted using this
789 subset with the reference list comprising all significantly differentially expressed genes between the
790 *Zmtml1tml2* plants and segregating wild-type siblings. Enriched parent GO terms that were
791 overrepresented at FDR <0.005 and a corrected P value of ≤ 0.05 were plotted in R using ggplot2 [100].
792
793 *Statistical Analysis*
794 Statistical tests were undertaken using R Studio. One-way ANOVA tests were performed for analyses
795 involving more than two groups, followed by Tukey's HSD post-hoc testing if the ANOVA *p* value was
796 <0.05. Details of ANOVA analyses are summarized in Supplementary File 13.
797
798 *Data access*
799 All read datasets were deposited at the NCBI sequence read archive (http://www.ncbi.nlm.nih.gov/sra)
800 under accession numbers SRSxxxxx–SRSxxxxx inclusive.
801
802 **LIST OF SUPPLEMENTARY MATERIAL**
803 **Figure S1.** WIP6 protein alignment.
804 **Figure S2.** Spatial localization of WIP6 transcripts in different grass species.

805 **Figure S3.** WIP6 loss of function alleles in maize and setaria.
806 **Figure S4.** Transcription factor expression profiles in maize shoots.
807 **Figure S5.** Transgenic rice lines expressing *ZmTML* or *OsTML* could not be generated..
808 **Figure S6.** Venation defects are restricted to leaves in *Ostml* mutants.
809 **Table S1.** Primer sequences used for cloning *OsTML* complementation constructs.
810 **File S1.** List of sequences in the WIP orthogroup.
811 **File S2.** Alignment of 379 WIP protein sequences used to infer the phylogeny in Figure 1A.
812 **File S3.** IQTreefile of WIP phylogeny presented in Figure 1A.
813 **File S4.** Subset of 17 WIP6 protein sequences used to infer the phylogeny in Figure 1B.
814 **File S5.** Alignment of 17 WIP6 protein sequences (illustrated in Figure S1A) and used to infer the
815 phylogeny in Figure 1B.
816 **File S6.** IQTreefile of WIP6 phylogeny presented in Figure 1B.
817 **File S7.** Subset of 50 WIP6 protein sequences from 41 species used for the alignment in Figure S1B.
818 **File S8.** List of genes that are differentially regulated in shoot apices of wild-type and *Zmtml1tml2*
819 mutants.
820 **File S9.** Levels of transcripts encoding candidate regulators of Kranz anatomy in wild-type and
821 *Zmtml1tml2* mutant shoot apices.
822 **File S10.** Genes encoding cytokinin pathway components that are differentially regulated in wild-type
823 and *Zmtml1tml2* mutant shoot apices.
824 **File S11.** Genes encoding auxin pathway associated genes that are differentially regulated in wild-type
825 and *Zmtml1tml2* mutant shoot apices.
826 File S12. Alignment of *ZmTML1* promoter with the domesticated version used in transformation
827 constructs.
828 **File S13**. Data and statistical analyses supporting main figures.
829

830 **AUTHOR CONTRIBUTIONS**

831 D.V., C.P., M.Z., O.S. and J.A.L. conceived and designed the experiments; J.A.L. carried out the
832 phylogenetic analysis (Figs. 1 & S1), O.S. performed *in situ* hybridizations (Figs. 2 & S2); C.P. and S.B.
833 generated the molecular cartography data (Figs. 2, S2 & S4), M.Z. performed the transcriptome
834 analysis (Figs. 4 & S4), D.V. carried out all of the remaining experiments. D.V., C.P., M.Z. and J.A.L.
835 analysed the data. D.V. and J.A.L. wrote the first draft of the manuscript and all authors contributed to
836 the final version.
837

838 **ACKNOWLEDGEMENTS**

839 The authors thank Laurens Pauwels and the VIB team for maize transformation; David Emms for
840 providing the WIP orthogroup sequences; Mara Schuler for making the *ZmUBI*$_{pro}$*:ZmTML* construct;
841 John Baker for plant photography; Roxaana Clayton, Julie Bull, Lizzie Jamison and Nina Johnson for

technical support; Tom Hughes, Sophie Johnson, Tina Schreier, Sovanna Tan and Steve Kelly for discussion throughout the experimental work and during manuscript preparation.

COMPETING INTERESTS

D.V. and J.A.L. have a pending patent application (PCT/IB2020/056992) related to some of the reported results.

FUNDING

This research was funded by the Bill and Melinda Gates Foundation C_4 Rice grant awarded to the University of Oxford (2015-2019 (OPP1129902) and 2019-2024 (INV-002970).

856 **REFERENCES**

857 1. Meinhardt, H. (2008). Models of Biological Pattern Formation: From Elementary Steps to the
858 Organization of Embryonic Axes. In Current Topics in Developmental Biology, S. Schnell, P.K.
859 Maini, S.A. Newman, and T.J. Newman, eds. (Academic Press), pp. 1-63.
860 https://doi.org/10.1016/S0070-2153(07)81001-5.
861 2. Kuhlemeier, C. (2007). Phyllotaxis. Trends Plant Sci *12*, 143-150.
862 https://doi.org/10.1016/j.tplants.2007.03.004.
863 3. Perico, C., Tan, S., and Langdale, J.A. (2022). Developmental regulation of leaf venation
864 patterns: monocot versus eudicots and the role of auxin. New Phytologist *234*, 783-803.
865 10.1111/nph.17955.
866 4. Roth-Nebelsick, A., Uhl, D., Mosbrugger, V., and Kerp, H. (2001). Evolution and function of leaf
867 venation architecture: A review. Ann Bot-London *87*, 553-566. 10.1006/anbo.2001.1391.
868 5. Sack, L., and Scoffoni, C. (2013). Leaf venation: structure, function, development, evolution,
869 ecology and applications in the past, present and future. New Phytologist *198*, 983-1000.
870 10.1111/nph.12253.
871 6. Jouannet, V., Brackmann, K., and Greb, T. (2015). (Pro)cambium formation and proliferation:
872 two sides of the same coin? Curr Opin Plant Biol *23*, 54-60.
873 https://doi.org/10.1016/j.pbi.2014.10.010.
874 7. Linh, N.M., and Scarpella, E. (2022). Leaf vein patterning is regulated by the aperture of
875 plasmodesmata intercellular channels. PLOS Biology *20*, e3001781.
876 10.1371/journal.pbio.3001781.
877 8. Sawchuk, M.G., Edgar, A., and Scarpella, E. (2013). Patterning of leaf vein networks by
878 convergent auxin transport pathways. PLoS Genet *9*, e1003294.
879 10.1371/journal.pgen.1003294.
880 9. Govindaraju, P., Verna, C., Zhu, T., and Scarpella, E. (2020). Vein patterning by tissue-specific
881 auxin transport. Development *147*. 10.1242/dev.187666.
882 10. Scarpella, E. (2023). Axes and polarities in leaf vein formation. Plant Physiology, kiad321.
883 10.1093/plphys/kiad321.
884 11. Mattsson, J., Ckurshumova, W., and Berleth, T. (2003). Auxin signaling in Arabidopsis leaf
885 vascular development. Plant Physiol *131*, 1327-1339. 10.1104/pp.013623.
886 12. Wenzel, C.L., Schuetz, M., Yu, Q., and Mattsson, J. (2007). Dynamics of MONOPTEROS and
887 PIN-FORMED1 expression during leaf vein pattern formation in Arabidopsis thaliana. Plant J
888 *49*, 387-398. 10.1111/j.1365-313X.2006.02977.x.
889 13. Donner, T.J., Sherr, I., and Scarpella, E. (2009). Regulation of preprocambial cell state
890 acquisition by auxin signaling in Arabidopsis leaves. Development *136*, 3235-3246.
891 10.1242/dev.037028.
892 14. Sawchuk, M.G., Head, P., Donner, T.J., and Scarpella, E. (2007). Time-lapse imaging of
893 Arabidopsis leaf development shows dynamic patterns of procambium formation. New Phytol
894 *176*, 560-571. 10.1111/j.1469-8137.2007.02193.x.

895 15. Marcos, D., and Berleth, T. (2014). Dynamic auxin transport patterns preceding vein formation
896 revealed by live-imaging of Arabidopsis leaf primordia. Front Plant Sci *5*, 235.
897 10.3389/fpls.2014.00235.
898 16. Sharman, B. (1942). Developmental anatomy of the shoot of Zea mays L. Ann Bot-London.
899 17. Russell, S.H., and Evert, R.F. (1985). Leaf Vasculature in Zea-Mays-L. Planta *164*, 448-458.
900 Doi 10.1007/Bf00395960.
901 18. Sedelnikova, O.V., Hughes, T.E., and Langdale, J.A. (2018). Understanding the genetic basis
902 of C_4 Kranz anatomy with a view to engineering C_3 crops. Annual Review of Genetics *52*, 249-
903 270. 10.1146/annurev-genet-120417-031217.
904 19. Sage, R.F., Christin, P.-A., and Edwards, E.J. (2011). The C4 plant lineages of planet Earth. J
905 Exp Bot.
906 20. Sharman, B.C., and Hitch, P.A. (1967). Initiation of Procambial Strands in Leaf Primordia of
907 Bread Wheat, Triticum aestivum L. Ann Bot-London *31*, 229-243.
908 10.1093/oxfordjournals.aob.a084135.
909 21. Sakaguchi, J., and Fukuda, H. (2008). Cell differentiation in the longitudinal veins and formation
910 of commissural veins in rice (Oryza sativa) and maize (Zea mays). Journal of Plant Research.
911 Springer.
912 22. Johnston, R., Leiboff, S., and Scanlon, M.J. (2015). Ontogeny of the sheathing leaf base in
913 maize (Zea mays). New Phytol *205*, 306-315. 10.1111/nph.13010.
914 23. Lee, B.H., Johnston, R., Yang, Y., Gallavotti, A., Kojima, M., Travencolo, B.A., Costa Lda, F.,
915 Sakakibara, H., and Jackson, D. (2009). Studies of aberrant phyllotaxy1 mutants of maize
916 indicate complex interactions between auxin and cytokinin signaling in the shoot apical
917 meristem. Plant Physiol *150*, 205-216. 10.1104/pp.109.137034.
918 24. Robil, J.M., and McSteen, P. (2023). Hormonal control of medial-lateral growth and vein
919 formation in the maize leaf. New Phytol *238*, 125-141. 10.1111/nph.18625.
920 25. O'Connor, D.L., Runions, A., Sluis, A., Bragg, J., Vogel, J.P., Prusinkiewicz, P., and Hake, S.
921 (2014). A division in PIN-mediated auxin patterning during organ initiation in grasses. PLoS
922 Comput Biol *10*, e1003447. 10.1371/journal.pcbi.1003447.
923 26. Scarpella, E., Rueb, S., Boot, K.J., Hoge, J.H., and Meijer, A.H. (2000). A role for the rice
924 homeobox gene Oshox1 in provascular cell fate commitment. Development *127*, 3655-3669.
925 27. Appelhagen, I., Huep, G., Lu, G.-H., Strompen, G., Weisshaar, B., and Sagasser, M. (2010).
926 Weird fingers: Functional analysis of WIP domain proteins. FEBS Letters *584*, 3116-3122.
927 https://doi.org/10.1016/j.febslet.2010.06.007.
928 28. Wang, P., Kelly, S., Fouracre, J.P., and Langdale, J.A. (2013). Genome-wide transcript analysis
929 of early maize leaf development reveals gene cohorts associated with the differentiation of C4
930 Kranz anatomy. Plant J *75*, 656-670. 10.1111/tpj.12229.
931 29. Fouracre, J.P., Ando, S., and Langdale, J.A. (2014). Cracking the Kranz enigma with systems
932 biology. J Exp Bot. 2014/02/11 ed.

933 30. Emms, D.M., and Kelly, S. (2019). OrthoFinder: phylogenetic orthology inference for
934 comparative genomics. Genome Biology *20*, 238. 10.1186/s13059-019-1832-y.
935 31. Sagasser, M., Lu, G.H., Hahlbrock, K., and Weisshaar, B. (2002). A. thaliana TRANSPARENT
936 TESTA 1 is involved in seed coat development and defines the WIP subfamily of plant zinc
937 finger proteins. Genes Dev *16*, 138-149. 10.1101/gad.212702.
938 32. Petricka, J.J., Clay, N.K., and Nelson, T.M. (2008). Vein patterning screens and the defectively
939 organized tributaries mutants in Arabidopsis thaliana. The Plant Journal *56*, 251-263.
940 https://doi.org/10.1111/j.1365-313X.2008.03595.x.
941 33. Du, Y., Roldan, M.V.G., Haraghi, A., Haili, N., Izhaq, F., Verdenaud, M., Boualem, A., and
942 Bendahmane, A. (2022). Spatially expressed WIP genes control Arabidopsis embryonic root
943 development. Nature Plants *8*, 635-645. 10.1038/s41477-022-01172-4.
944 34. Vlad, D., and Langdale, J.A. (2022). DEFECTIVELY ORGANIZED TRIBUTARIES 5 is not
945 required for leaf venation patterning in Arabidopsis thaliana. The Plant Journal *112*, 451-459.
946 https://doi.org/10.1111/tpj.15958.
947 35. Gaut, B.S. (2001). Patterns of chromosomal duplication in maize and their implications for
948 comparative maps of the grasses. Genome Res *11*, 55-66. 10.1101/gr.160601.
949 36. Englbrecht, C.C., Schoof, H., and Böhm, S. (2004). Conservation, diversification and expansion
950 of C2H2 zinc finger proteins in the Arabidopsis thaliana genome. BMC Genomics *5*, 39.
951 10.1186/1471-2164-5-39.
952 37. Kagale, S., and Rozwadowski, K. (2011). EAR motif-mediated transcriptional repression in
953 plants: an underlying mechanism for epigenetic regulation of gene expression. Epigenetics *6*,
954 141-146. 10.4161/epi.6.2.13627.
955 38. Ohta, M., Matsui, K., Hiratsu, K., Shinshi, H., and Ohme-Takagi, M. (2001). Repression
956 domains of class II ERF transcriptional repressors share an essential motif for active repression.
957 Plant Cell *13*, 1959-1968. 10.1105/tpc.010127.
958 39. Slewinski, T.L., Anderson, A.A., Price, S., Withee, J.R., Gallagher, K., and Turgeon, R. (2014).
959 Short-root1 plays a role in the development of vascular tissue and Kranz anatomy in maize
960 leaves. Mol Plant. Elsevier.
961 40. Slewinski, T.L., Anderson, A.A., Zhang, C., and Turgeon, R. (2012). Scarecrow plays a role in
962 establishing Kranz anatomy in maize leaves. Plant & Cell Physiology. 2012/11/07 ed.
963 41. Hughes, T.E., Sedelnikova, O.V., Wu, H., Becraft, P.W., and Langdale, J.A. (2019). Redundant
964 SCARECROW genes pattern distinct cell layers in roots and leaves of maize. Development
965 *146*, e177543. 10.1242/dev.177543.
966 42. Hughes, T.E., and Langdale, J.A. (2022). SCARECROW is deployed in distinct contexts during
967 rice and maize leaf development. Development *149*, e200410. 10.1242/dev.200410.
968 43. Hughes, T.E., Sedelnikova, O., Thomas, M., and Langdale, J.A. (2023). Mutations in NAKED-
969 ENDOSPERM IDD genes reveal functional interactions with SCARECROW during leaf
970 patterning in C4 grasses. PLoS Genet *19*, e1010715. 10.1371/journal.pgen.1010715.

971 44. Rodriguez, R.E., Mecchia, M.A., Debernardi, J.M., Schommer, C., Weigel, D., and Palatnik,
972 J.F. (2010). Control of cell proliferation in Arabidopsis thaliana by microRNA miR396.
973 Development *137*, 103-112. 10.1242/dev.043067.
974 45. Nelissen, H., Eeckhout, D., Demuynck, K., Persiau, G., Walton, A., van Bel, M., Vervoort, M.,
975 Candaele, J., De Block, J., Aesaert, S., et al. (2015). Dynamic Changes in ANGUSTIFOLIA3
976 Complex Composition Reveal a Growth Regulatory Mechanism in the Maize Leaf. Plant Cell
977 *27*, 1605-1619. 10.1105/tpc.15.00269.
978 46. Liu, W.Y., Lin, H.H., Yu, C.P., Chang, C.K., Chen, H.J., Lin, J.J., Lu, M.J., Tu, S.L., Shiu, S.H.,
979 Wu, S.H., et al. (2020). Maize ANT1 modulates vascular development, chloroplast
980 development, photosynthesis, and plant growth. Proc Natl Acad Sci U S A *117*, 21747-21756.
981 10.1073/pnas.2012245117.
982 47. Nelissen, H., Rymen, B., Jikumaru, Y., Demuynck, K., Van Lijsebettens, M., Kamiya, Y., Inzé,
983 D., and Beemster, G.T. (2012). A local maximum in gibberellin levels regulates maize leaf
984 growth by spatial control of cell division. Curr Biol *22*, 1183-1187. 10.1016/j.cub.2012.04.065.
985 48. De Vos, D., Nelissen, H., AbdElgawad, H., Prinsen, E., Broeckhove, J., Inzé, D., and Beemster,
986 G.T.S. (2020). How grass keeps growing: an integrated analysis of hormonal crosstalk in the
987 maize leaf growth zone. New Phytologist *225*, 2513-2525. https://doi.org/10.1111/nph.16315.
988 49. Muszynski, M.G., Moss-Taylor, L., Chudalayandi, S., Cahill, J., Del Valle-Echevarria, A.R.,
989 Alvarez-Castro, I., Petefish, A., Sakakibara, H., Krivosheev, D.M., Lomin, S.N., et al. (2020).
990 The Maize Hairy Sheath Frayed1 (Hsf1) Mutation Alters Leaf Patterning through Increased
991 Cytokinin Signaling[OPEN]. The Plant Cell *32*, 1501-1518. 10.1105/tpc.19.00677.
992 50. Ko, D., Kang, J., Kiba, T., Park, J., Kojima, M., Do, J., Kim, K.Y., Kwon, M., Endler, A., Song,
993 W.-Y., et al. (2014). Arabidopsis ABCG14 is essential for the root-to-shoot translocation of
994 cytokinin. Proceedings of the National Academy of Sciences *111*, 7150-7155.
995 10.1073/pnas.1321519111.
996 51. Vyroubalová, S., Václavíková, K., Turecková, V., Novák, O., Smehilová, M., Hluska, T.,
997 Ohnoutková, L., Frébort, I., and Galuszka, P. (2009). Characterization of new maize genes
998 putatively involved in cytokinin metabolism and their expression during osmotic stress in
999 relation to cytokinin levels. Plant Physiol *151*, 433-447. 10.1104/pp.109.142489.
1000 52. Lavy, M., and Estelle, M. (2016). Mechanisms of auxin signaling. Development *143*, 3226-3229.
1001 10.1242/dev.131870.
1002 53. Seo, M., Akaba, S., Oritani, T., Delarue, M., Bellini, C., Caboche, M., and Koshiba, T. (1998).
1003 Higher Activity of an Aldehyde Oxidase in the Auxin-Overproducing superroot1 Mutant
1004 ofArabidopsis thaliana1. Plant Physiology *116*, 687-693. 10.1104/pp.116.2.687.
1005 54. Przemeck, G.K., Mattsson, J., Hardtke, C.S., Sung, Z.R., and Berleth, T. (1996). Studies on the
1006 role of the Arabidopsis gene MONOPTEROS in vascular development and plant cell
1007 axialization. Planta *200*, 229-237. 10.1007/BF00208313.

1008 55. Hardtke, C.S., and Berleth, T. (1998). The Arabidopsis gene MONOPTEROS encodes a
1009 transcription factor mediating embryo axis formation and vascular development. EMBO Journal
1010 *17*, 1405-1411. 10.1093/emboj/17.5.1405.
1011 56. Parry, G., Ward, S., Cernac, A., Dharmasiri, S., and Estelle, M. (2006). The Arabidopsis
1012 SUPPRESSOR OF AUXIN RESISTANCE Proteins Are Nucleoporins with an Important Role in
1013 Hormone Signaling and Development. The Plant Cell *18*, 1590-1603. 10.1105/tpc.106.041566.
1014 57. Galli, M., Khakhar, A., Lu, Z., Chen, Z., Sen, S., Joshi, T., Nemhauser, J.L., Schmitz, R.J., and
1015 Gallavotti, A. (2018). The DNA binding landscape of the maize AUXIN RESPONSE FACTOR
1016 family. Nature Communications.
1017 58. Wang, P., Vlad, D., and Langdale, J.A. (2016). Finding the genes to build C4 rice. Curr Opin
1018 Plant Biol.
1019 59. Hibberd, J.M., Sheehy, J.E., and Langdale, J.A. (2008). Using C4 photosynthesis to increase
1020 the yield of rice-rationale and feasibility. Curr Opin Plant Biol. 2008/01/22 ed.
1021 60. Jones, V.A., and Dolan, L. (2017). MpWIP regulates air pore complex development in the
1022 liverwort Marchantia polymorpha. Development *144*, 1472-1476. 10.1242/dev.144287.
1023 61. Crawford, B.C.W., Ditta, G., and Yanofsky, M.F. (2007). The NTT Gene Is Required
1024 for Transmitting-Tract Development in Carpels of Arabidopsis thaliana. Current
1025 Biology *17*, 1101-1108. 10.1016/j.cub.2007.05.079.
1026 62. Crawford, B.C.W., Sewell, J., Golembeski, G., Roshan, C., Long, J.A., and Yanofsky, M.F.
1027 (2015). Genetic control of distal stem cell fate within root and embryonic meristems. Science
1028 *347*, 655-659. 10.1126/science.aaa0196.
1029 63. Diaz-Ramirez, D., Diaz-Garcia, U.S., Magdaleno-Garcia, G., Huep, G., Appelhagen, I.,
1030 Sagasser, M., and Marsch-Martinez, N. (2022). Expression and Functional Analyses of the WIP
1031 Gene Family in Arabidopsis. Plants (Basel) *11*. 10.3390/plants11152010.
1032 64. Roldan, M.V.G., Izhaq, F., Verdenaud, M., Eleblu, J., Haraghi, A., Sommard, V., Chambrier, P.,
1033 Latrasse, D., Jégu, T., Benhamed, M., et al. (2020). Integrative genome-wide analysis reveals
1034 the role of WIP proteins in inhibition of growth and development. Commun Biol *3*, 239.
1035 10.1038/s42003-020-0969-2.
1036 65. Ren, G., Li, L., Huang, Y., Wang, Y., Zhang, W., Zheng, R., Zhong, C., and Wang, X. (2018).
1037 GhWIP2, a WIP zinc finger protein, suppresses cell expansion in Gerbera hybrida by mediating
1038 crosstalk between gibberellin, abscisic acid, and auxin. New Phytologist *219*, 728-742.
1039 https://doi.org/10.1111/nph.15175.
1040 66. Liu, W.-Y., Yu, C.-P., Chang, C.-K., Chen, H.-J., Li, M.-Y., Chen, Y.-H., Shiu, S.-H., Ku, M.S.B.,
1041 Tu, S.-L., Lu, M.-Y.J., and Li, W.-H. (2022). Regulators of early maize leaf development inferred
1042 from transcriptomes of laser capture microdissection (LCM)-isolated embryonic leaf cells.
1043 Proceedings of the National Academy of Sciences *119*, e2208795119.
1044 10.1073/pnas.2208795119.

1045 67. Carland, F., and Nelson, T. (2009). CVP2- and CVL1-mediated phosphoinositide signaling as
1046 a regulator of the ARF GAP SFC/VAN3 in establishment of foliar vein patterns. The Plant
1047 Journal. Blackwell Publishing Ltd.
1048 68. Clay, N.K., and Nelson, T. (2005). Arabidopsis thickvein mutation affects vein thickness and
1049 organ vascularization, and resides in a provascular cell-specific spermine synthase involved in
1050 vein definition and in polar auxin transport. Plant Physiol *138*, 767-777.
1051 10.1104/pp.104.055756.
1052 69. Tsiantis, M., Brown, M.I., Skibinski, G., and Langdale, J.A. (1999). Disruption of auxin transport
1053 is associated with aberrant leaf development in maize. Plant Physiol *121*, 1163-1168.
1054 10.1104/pp.121.4.1163.
1055 70. Rizal, G., Thakur, V., Dionora, J., Karki, S., Wanchana, S., Acebron, K., Larazo, N., Garcia, R.,
1056 Mabilangan, A., Montecillo, F., et al. (2015). Two forward genetic screens for vein density
1057 mutants in sorghum converge on a cytochrome P450 gene in the brassinosteroid pathway. The
1058 Plant Journal.
1059 71. Sakamoto, T., Sakakibara, H., Kojima, M., Yamamoto, Y., Nagasaki, H., Inukai, Y., Sato, Y.,
1060 and Matsuoka, M. (2006). Ectopic expression of KNOTTED1-like homeobox protein induces
1061 expression of cytokinin biosynthesis genes in rice. Plant Physiol.
1062 72. Smillie, I.R., Pyke, K.A., and Murchie, E.H. (2012). Variation in vein density and mesophyll cell
1063 architecture in a rice deletion mutant population. Journal Experimental Botany *63*, 4563-4570.
1064 10.1093/jxb/ers142.
1065 73. Feldman, A.B., Murchie, E.H.E., Leung, H., Baraoidan, M., Coe, R., Yu, S.-M.S.-M., Lo, S.-F.,
1066 Quick, W.P., Sage, T., Sage, R., et al. (2014). Increasing leaf vein density by mutagenesis:
1067 laying the foundations for C4 rice. In K. Wu, ed. PLoS ONE. Public Library of Science.
1068 74. Qi, J., Qian, Q., Bu, Q., Li, S., Chen, Q., Sun, J., Liang, W., Zhou, Y., Chu, C., Li, X., et al.
1069 (2008). Mutation of the rice Narrow leaf1 gene, which encodes a novel protein, affects vein
1070 patterning and polar auxin transport. Plant Physiol *147*, 1947-1959. 10.1104/pp.108.118778.
1071 75. Scarpella, E., Rueb, S., and Meijer, A.H. (2003). The RADICLELESS1 gene is required for
1072 vascular pattern formation in rice. Development *130*, 645-658. 10.1242/dev.00243.
1073 76. Goodstein, D.M., Shu, S., Howson, R., Neupane, R., Hayes, R.D., Fazo, J., Mitros, T., Dirks,
1074 W., Hellsten, U., Putnam, N., and Rokhsar, D.S. (2012). Phytozome: a comparative platform
1075 for green plant genomics. Nucleic Acids Res *40*, D1178-1186. 10.1093/nar/gkr944.
1076 77. Collingridge, P.W., and Kelly, S. (2012). MergeAlign: improving multiple sequence alignment
1077 performance by dynamic reconstruction of consensus multiple sequence alignments. BMC
1078 Bioinformatics *13*, 117. 10.1186/1471-2105-13-117.
1079 78. Tamura, K., Stecher, G., and Kumar, S. (2021). MEGA11: Molecular Evolutionary Genetics
1080 Analysis Version 11. Molecular Biology and Evolution *38*, 3022-3027.
1081 10.1093/molbev/msab120.

1082 79. Trifinopoulos, J., Nguyen, L.T., von Haeseler, A., and Minh, B.Q. (2016). W-IQ-TREE: a fast
1083 online phylogenetic tool for maximum likelihood analysis. Nucleic Acids Res *44*, W232-235.
1084 10.1093/nar/gkw256.
1085 80. Letunic, I., and Bork, P. (2021). Interactive Tree Of Life (iTOL) v5: an online tool for phylogenetic
1086 tree display and annotation. Nucleic Acids Research *49*, W293-W296. 10.1093/nar/gkab301.
1087 81. Katoh, K., Kuma, K.-i., Toh, H., and Miyata, T. (2005). MAFFT version 5: improvement in
1088 accuracy of multiple sequence alignment. Nucleic Acids Research *33*, 511-518.
1089 10.1093/nar/gki198.
1090 82. Schuler, M.L., Sedelnikova, O.V., Walker, B.J., Westhoff, P., and Langdale, J.A. (2018).
1091 SHORTROOT-Mediated Increase in Stomatal Density Has No Impact on Photosynthetic
1092 Efficiency. Plant Physiol *176*, 757-772. 10.1104/pp.17.01005.
1093 83. Glenn, P., Woods, D.P., Zhang, J., Gabay, G., Odle, N., and Dubcovsky, J. (2023). Wheat
1094 bZIPC1 interacts with FT2 and contributes to the regulation of spikelet number per spike.
1095 Theoretical and Applied Genetics *136*, 237. 10.1007/s00122-023-04484-x.
1096 84. Pachitariu, M., and Stringer, C. (2022). Cellpose 2.0: how to train your own model. Nat Methods
1097 *19*, 1634-1641. 10.1038/s41592-022-01663-4.
1098 85. Concordet, J.-P., and Haeussler, M. (2018). CRISPOR: intuitive guide selection for
1099 CRISPR/Cas9 genome editing experiments and screens. Nucleic Acids Research *46*, W242-
1100 W245. 10.1093/nar/gky354.
1101 86. Weber, E., Engler, C., Gruetzner, R., Werner, S., and Marillonnet, S. (2011). A modular cloning
1102 system for standardized assembly of multigene constructs. PLoS One *6*, e16765.
1103 10.1371/journal.pone.0016765.
1104 87. Ma, X., Zhang, Q., Zhu, Q., Liu, W., Chen, Y., Qiu, R., Wang, B., Yang, Z., Li, H., Lin, Y., et al.
1105 (2015). A Robust CRISPR/Cas9 System for Convenient, High-Efficiency Multiplex Genome
1106 Editing in Monocot and Dicot Plants. Mol Plant *8*, 1274-1284.
1107 https://doi.org/10.1016/j.molp.2015.04.007.
1108 88. Kim, C.M., and Dolan, L. (2016). ROOT HAIR DEFECTIVE SIX-LIKE Class I Genes Promote
1109 Root Hair Development in the Grass Brachypodium distachyon. In L.-J. Qu, ed. PLOS Genetics.
1110 89. Ricci, W.A., Lu, Z., Ji, L., Marand, A.P., Ethridge, C.L., Murphy, N.G., Noshay, J.M., Galli, M.,
1111 Mejía-Guerra, M.K., Colomé-Tatché, M., et al. (2019). Widespread long-range cis-regulatory
1112 elements in the maize genome. Nature Plants *5*, 1237-1249. 10.1038/s41477-019-0547-0.
1113 90. Lu, Z., Marand, A.P., Ricci, W.A., Ethridge, C.L., Zhang, X., and Schmitz, R.J. (2019). The
1114 prevalence, evolution and chromatin signatures of plant regulatory elements. Nature Plants *5*,
1115 1250-1259. 10.1038/s41477-019-0548-z.
1116 91. Toki, S., Hara, N., Ono, K., Onodera, H., Tagiri, A., Oka, S., and Tanaka, H. (2006). Early
1117 infection of scutellum tissue with Agrobacterium allows high-speed transformation of rice. Plant
1118 Journal.

1119 92. Dobin, A., Davis, C.A., Schlesinger, F., Drenkow, J., Zaleski, C., Jha, S., Batut, P., Chaisson,
1120 M., and Gingeras, T.R. (2013). STAR: ultrafast universal RNA-seq aligner. Bioinformatics *29*,
1121 15-21. 10.1093/bioinformatics/bts635.
1122 93. Patro, R., Duggal, G., Love, M.I., Irizarry, R.A., and Kingsford, C. (2017). Salmon provides fast
1123 and bias-aware quantification of transcript expression. Nat Methods *14*, 417-419.
1124 10.1038/nmeth.4197.
1125 94. Love, M.I., Huber, W., and Anders, S. (2014). Moderated estimation of fold change and
1126 dispersion for RNA-seq data with DESeq2. Genome Biology *15*, 550. 10.1186/s13059-014-
1127 0550-8.
1128 95. Matthes, M.S., Best, N.B., Robil, J.M., Malcomber, S., Gallavotti, A., and McSteen, P. (2019).
1129 Auxin EvoDevo: Conservation and Diversification of Genes Regulating Auxin Biosynthesis,
1130 Transport, and Signaling. Mol Plant *12*, 298-320. 10.1016/j.molp.2018.12.012.
1131 96. The Gene Ontology, C., Aleksander, S.A., Balhoff, J., Carbon, S., Cherry, J.M., Drabkin, H.J.,
1132 Ebert, D., Feuermann, M., Gaudet, P., Harris, N.L., et al. (2023). The Gene Ontology
1133 knowledgebase in 2023. Genetics *224*, iyad031. 10.1093/genetics/iyad031.
1134 97. Thomas, P.D., Ebert, D., Muruganujan, A., Mushayahama, T., Albou, L.-P., and Mi, H. (2022).
1135 PANTHER: Making genome-scale phylogenetics accessible to all. Protein Science *31*, 8-22.
1136 https://doi.org/10.1002/pro.4218.
1137 98. The UniProt, C. (2023). UniProt: the Universal Protein Knowledgebase in 2023. Nucleic Acids
1138 Research *51*, D523-D531. 10.1093/nar/gkac1052.
1139 99. Yilmaz, A., Nishiyama, M.Y., Jr., Fuentes, B.G., Souza, G.M., Janies, D., Gray, J., and
1140 Grotewold, E. (2009). GRASSIUS: A Platform for Comparative Regulatory Genomics across
1141 the Grasses Plant Physiology *149*, 171-180. 10.1104/pp.108.128579.
1142 100. Wickham, H. (2009). ggplot2. Elegant Graphics for Data Analysis.

1143

1144

1145 **FIGURE LEGENDS**

1146

1147 **Figure 1. Monocot WIP6 orthologs contain a conserved N terminal EAR domain. A)** Maximum
1148 Likelihood phylogeny of WIP proteins in land plants, rooted with the single WIP gene from *Marchantia*
1149 *polymorpha* (*MpWIP*). Six WIP genes are present in *Arabidopsis thaliana,* with four clades identified in
1150 basal angiosperms (WIP1, WIP3, WIP2,4,5 and WIP6), and two clades (WIP6 and WIP1-5) identified
1151 in all vascular plant lineages. Maize has two genes in the WIP6 clade. **B)** Maximum likelihood
1152 phylogeny of WIP6 proteins from representative eudicots (orange shading) and monocots (pink
1153 shading), rooted with the bryophyte clade. Bootstrap values are indicated below branches. **C)**
1154 Schematic representation of monocot WIP6 genes showing 5' and 3' UTRs (black lines) plus two exons
1155 (rectangles) separated by an intron (^). The arrow indicates the direction of transcription, the conserved
1156 EAR domain (grey box) and the C2H2 zinc finger region (black boxes) are highlighted. The protein
1157 alignment illustrates the amino acid residues in the conserved protein domains. The LxLxL type EAR
1158 motif present in monocot WIP6 proteins is not present in eudicot proteins (Figure S1). A WIP domain
1159 (in bold) and up to four zinc fingers (ZF) are predicted. The ZFs are highlighted in black with the zinc
1160 binding residues in red and the nuclear localization signal (NLS) is highlighted in yellow.

1161

1162 **Figure 2. WIP6 genes are expressed in dividing procambial cells in maize leaf primordia. A, B)**
1163 Schematics of cellular arrangements in a P4 primordium (A) and an expanded leaf (B). Different vein
1164 and cell-types are indicated. **C, D)** *In situ* hybridization of *ZmWIP6A* (Zm00001d020037) (C) and
1165 *ZmWIP6B* (Zm00001d005566) (D) transcripts to P3-P5 leaf primordia of maize. Plastochron stages
1166 are as indicated. Scale bars = 100μm **E)** Annotated image of a section hybridized with *ZmWIP6A*. The
1167 P5 primordium is outlined in purple and ground meristem cells are outlined in yellow. Four different
1168 stages of vein development are highlighted. The white arrowhead marks a procambial initial, which can
1169 only be distinguished from the surrounding ground meristem cells by the presence of *ZmWIP6A*
1170 transcripts. The green cells denote early dividing procambial centres, with the black arrowhead marking
1171 the more advanced stage. Black cells surround fully differentiated veins. *ZmWIP6A* transcripts are
1172 detected in the procambial initial and in the early dividing procambium but are absent once the
1173 developing vein comprises more than four or five cells (black arrowhead). Scale bar = 50μm. **F, G)**
1174 Molecular cartography showing accumulation of *ZmWIP6A* (Zm00001d020037) (blue dots in F, G) and
1175 *ZmWIP6B* (Zm00001d005566) (orange dots in G) transcripts in the shoot apical meristem and P1-P5
1176 leaf primordia of maize. The purple line indicates the meristem, green dotted line the P0 primordium,
1177 orange line the P1 primordium and pink line the P2 primordium. White arrows indicate developing
1178 intermediate veins in the P5 leaf sheath tissue. Scale bar = 100μm.

1179

1180 **Figure 3. Loss of ZmWIP6A function leads to the formation of too many lateral veins in the**
1181 **maize leaf. A)** Gene models of *ZmWIP6A* and *ZmWIP6B* showing 5' and 3' UTRs (black lines) plus
1182 two exons (rectangles) separated by an intron (^). The arrow indicates the direction of transcription,
1183 the conserved EAR domain (grey box), the C2H2 zinc finger region (black boxes) and the sgRNA target

1184 sites (red) are highlighted. The sgRNA sequences used for CRISPR/Cas9 mediated mutagenesis are
1185 as shown, with the PAM sequences in italics. **B)** Allelic composition of wild-type (WT) and four T1
1186 maize lines. Mutant alleles are highlighted in pink and base insertions are highlighted in blue. One line
1187 (I20) was heteroallelic at both loci, one (J3) was heterozygous at both loci and the other two were
1188 heterozygous at one locus and wild-type at the other. **C)** Transverse sections of WT and mutant leaves
1189 showing vein numbers and types. In each case samples were taken from the 5th leaf in the region
1190 between laterals 2 and 4, with lateral 1 being the closest to the midvein. Asterisks indicate lateral veins,
1191 diamonds indicate ectopic lateral veins. Scale bars = 100µm. **D, E)** Quantification of the number of
1192 each vein type (D) and of total vein number (E) across the entire medio-lateral axis of the 5th leaf. 'Other
1193 rank 1 veins' are those which only have sclerenchyma on the adaxial or abaxial side but not both. N=5
1194 for *Zmwip6B_m1*, *Zmwip6A_m2* null segregant and *Zmwip6B_m1* null segregant, N=4 for
1195 *Zmwip6A_m2* and N=2 for the double homozygous *Zmwip6A_m1/Zmwip6B_m1* mutant. Statistical
1196 significance was determined using a one way ANOVA followed by a Tukey's test. **F-I)** Transverse
1197 sections of null segregant (F, H) and *Zmwip6A_m2* mutant (G, I) P4 primordia at the base (F, G) and
1198 in the middle (H, I) of the primordium. Midveins are highlighted in blue and lateral veins (both normal
1199 and ectopic) are highlighted in green. Orange arrows point to developing intermediate veins. Scale
1200 bars = 100µm. **J, K)** Cleared fragments of leaf 7 stained with Safranin showing the junction of leaf
1201 sheath and blade in null segregant (J) and *Zmwip6A_m2* (K) mutant leaves. Orange arrows point to a
1202 rank 1 intermediate with abaxial and adaxial sclerenchyma in (J) and an ectopic lateral in the equivalent
1203 position in (K). Yellow asterisks are positioned at transverse veins. Scale bar = 3mm.
1204
1205 **Figure 4. Evidence of auxin and cytokinin pathway perturbations in *Zmtml1tml2* mutant**
1206 **transcriptomes. A)** Overrepresentation analysis (ORA) of significantly different transcript levels (L2FC
1207 >1; $p \leq 0.05$) in *Zmtml1tml2* mutant apices as compared to corresponding segregating wild-type
1208 siblings, using data either from the whole transcriptome or from the subset annotated as transcription
1209 factors. Down- and up-regulated components are as indicated and the fold-enrichment in each case is
1210 shown by the size of the bubble. **B)** Log2fold difference in levels of transcript encoding auxin and
1211 cytokinin pathway components in *Zmtml1tml2* mutant apices as compared to corresponding
1212 segregating wild-type siblings. For each pathway step, the genes with significantly different transcript
1213 levels (L2FC ± 1; $p \leq 0.05$) are labeled.

1214 **Figure 5. Ectopic lateral vein formation in *Ostml* mutants of rice cannot be complemented by**
1215 ***OsTML* because transgene expression is suppressed. A)** Gene model of *OsTML* showing 5' and
1216 3' UTRs (black lines) plus two exons (rectangles) separated by an intron (^). The arrow indicates the
1217 direction of transcription, the conserved EAR domain (grey box), the C2H2 zinc finger region (black
1218 boxes) and the sgRNA target sites (red) are highlighted. The sgRNA sequences used for
1219 CRISPR/Cas9 mediated mutagenesis are as shown, with the PAM sequences in italics. **B)** Allelic
1220 composition of wild-type (WT) and five mutant rice lines. Base insertions are highlighted in red. **C)**
1221 Transverse sections of null segregant and *Ostml_m4* mutant leaves (flag leaf minus 1). Asterisks

1222 indicate lateral veins. Scale bar = 700 µm. **D)** Schematics of 5 transgenes used to complement *Ostml*
1223 mutants. Scale bar = ~1 kb. **E)** Transverse sections of leaf 7 from *Ostml_m3.1* mutant lines that were
1224 transformed with construct 2 from (D) and were germinated in the presence or absence of 50 mgL^{-1} 5
1225 aza-cytidine. Asterisks indicate lateral veins. Scale bar = 300 µm.

1226 **Figure 6. Venation defects in *Ostml* mutant leaves increase total vascular volume and alter**
1227 **bundle sheath cell dimensions. A)** Whole plant phenotype of three independent *Ostml* mutant lines
1228 and respective null segregant siblings. Lines were selected from F2 populations that had been
1229 generated by backcrossing transgene free T1 mutants to Kitaake and then self-pollinating the resultant
1230 BCF1 progeny. Scale bar = 10 cm. **B)** Transverse sections imaged between the midvein and the leaf
1231 margin of flag leaf minus 1 (left panel) and from the midvein to the position corresponding to the first
1232 adjacent lateral vein in wild-type (WT) of leaf 4 (right panel). Asterisks indicate lateral veins. Scale bars
1233 = 1 mm (left panel); 200 µm (right panel). **C-E)** Quantification of lateral vein numbers (C), intermediate
1234 vein numbers (D) and vein density (E) in leaf 7 of WT and mutant plants. n = 5 for each genotype;
1235 different letters indicate statistically different groups as determined using a one-way ANOVA followed
1236 by a Tukey's test (p value ≤ 0.05); see Supplementary File 13 for raw data. **F)** Paradermal images of
1237 the 7th leaf of WT and mutant plants, imaged in the middle of the blade. Lateral (L) and intermediate
1238 (i) veins are indicated. The longest bundle sheath cell around each vein in the field of view is outlined
1239 by a white box. Scale bar = 100 µm. **G)** Quantification of bundle sheath cell length around lateral
1240 (including ectopic laterals) and intermediate veins of WT and mutant leaves. n = 4 leaf samples and
1241 82/145 cells around L/i veins for WT; 3 leaf samples and 96/114, 45/44 and 130/130 cells for
1242 *Ostml_m3.1, _m3,3* and *_m4* mutants respectively. Different letters indicate statistically different
1243 groups as determined using a one-way ANOVA followed by a Tukey's test (p value ≤ 0.05); see
1244 Supplementary File 13 for raw data. **H)** Quantification of bundle sheath cells numbers around lateral
1245 (L), ectopic lateral (EL) and intermediate (i) veins in wild type and mutant plants. Different letters
1246 indicate statistically different groups as determined using a one-way ANOVA followed by a Tukey's test
1247 (p value ≤ 0.05); see Supplementary File 13 for raw data. Median values for bundle sheath length,
1248 number of bundle sheath cells and total vein numbers per leaf were used to estimate total number of
1249 bundle sheath cells and percentage increase in number in a leaf unit of 5 mm wide and 1 mm long.
1250

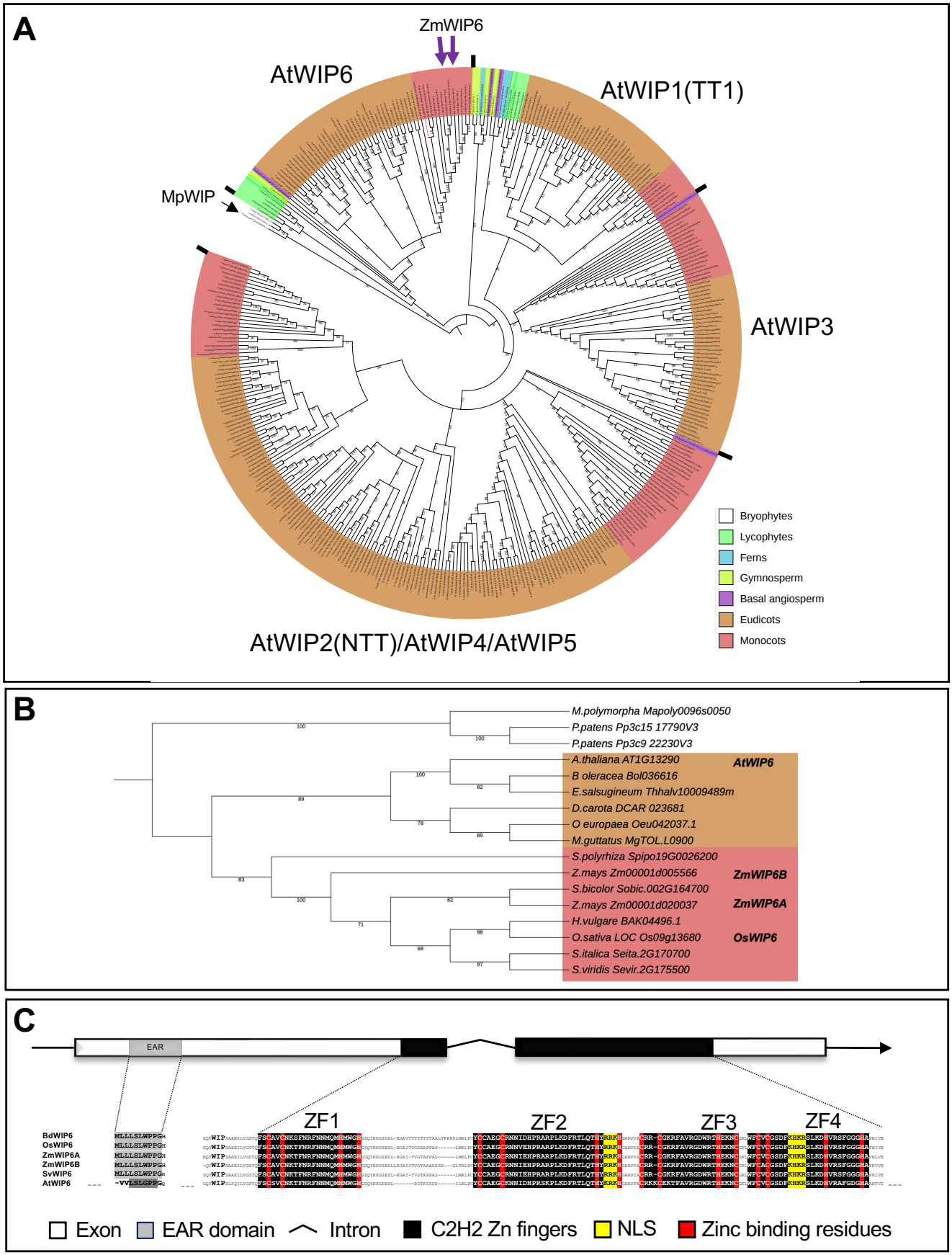

Figure 1. Monocot WIP6 orthologs contain a conserved N terminal EAR domain. A) Maximum Likelihood phylogeny of WIP proteins in land plants, rooted with the single WIP gene from *Marchantia polymorpha* (*MpWIP*). Six WIP genes are present in *Arabidopsis thaliana,* with four clades identified in basal angiosperms (WIP1, WIP3, WIP2,4,5 and WIP6), and two clades (WIP6 and WIP1-5) identified in all vascular plant lineages. Maize has two genes in the WIP6 clade. **B)** Maximum likelihood phylogeny of WIP6 proteins from representative eudicots (orange shading) and monocots (pink shading), rooted with the bryophyte clade. Bootstrap values are indicated below branches. **C)** Schematic representation of monocot WIP6 genes showing 5' and 3' UTRs (black lines) plus two exons (rectangles) separated by an intron (^). The arrow indicates the direction of transcription, the conserved EAR domain (grey box) and the C2H2 zinc finger region (black boxes) are highlighted. The protein alignment illustrates the amino acid residues in the conserved protein domains. The LxLxL type EAR motif present in monocot WIP6 proteins is not present in eudicot proteins (Figure S1). A WIP domain (in bold) and up to four zinc fingers (ZF) are predicted. The ZFs are highlighted in black with the zinc binding residues in red and the nuclear localization signal (NLS) is highlighted in yellow.

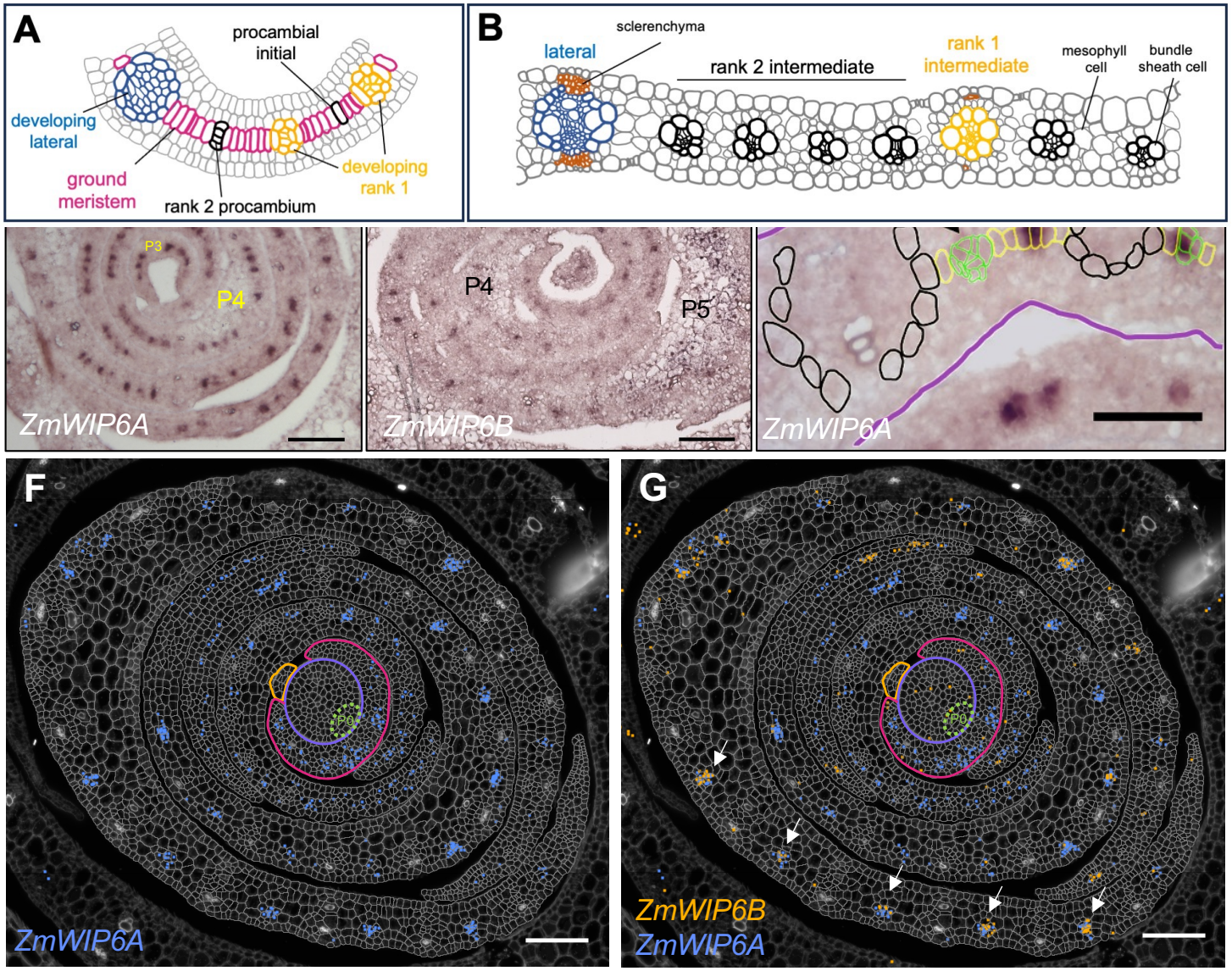

Figure 2. WIP6 genes are expressed in dividing procambial cells in maize leaf primordia. A, B) Schematics of cellular arrangements in a P4 primordium (A) and an expanded leaf (B). Different vein and cell-types are indicated. **C, D)** *In situ* hybridization of *ZmWIP6A* (Zm00001d020037) (C) and *ZmWIP6B* (Zm00001d005566) (D) transcripts to P3-P5 leaf primordia of maize. Plastochron stages are as indicated. Scale bars = 100μm **E)** Annotated image of a section hybridized with *ZmWIP6A*. The P5 primordium is outlined in purple and ground meristem cells are outlined in yellow. Four different stages of vein development are highlighted. The white arrowhead marks a procambial initial, the green cells denote early dividing procambial centres, with the black arrowhead marking the more advanced stage. Black cells surround fully differentiated veins. *ZmWIP6A* transcripts are detected in the procambial initial and in the early dividing procambium but are absent once the developing vein comprises more than four or five cells (black arrowhead). Scale bar = 50μm **F, G)** Molecular cartography showing accumulation of *ZmWIP6A* (Zm00001d020037) (blue dots in F, G) and *ZmWIP6B* (Zm00001d005566) (orange dots in G) transcripts in the shoot apical meristem and P1-P5 leaf primordia of maize. The purple line indicates the meristem, green dotted line the P0 primordium, orange line the P1 primordium and pink line the P2 primordium. White arrows indicate developing intermediate veins in the P5 leaf sheath tissue. Scale bar = 100μm.

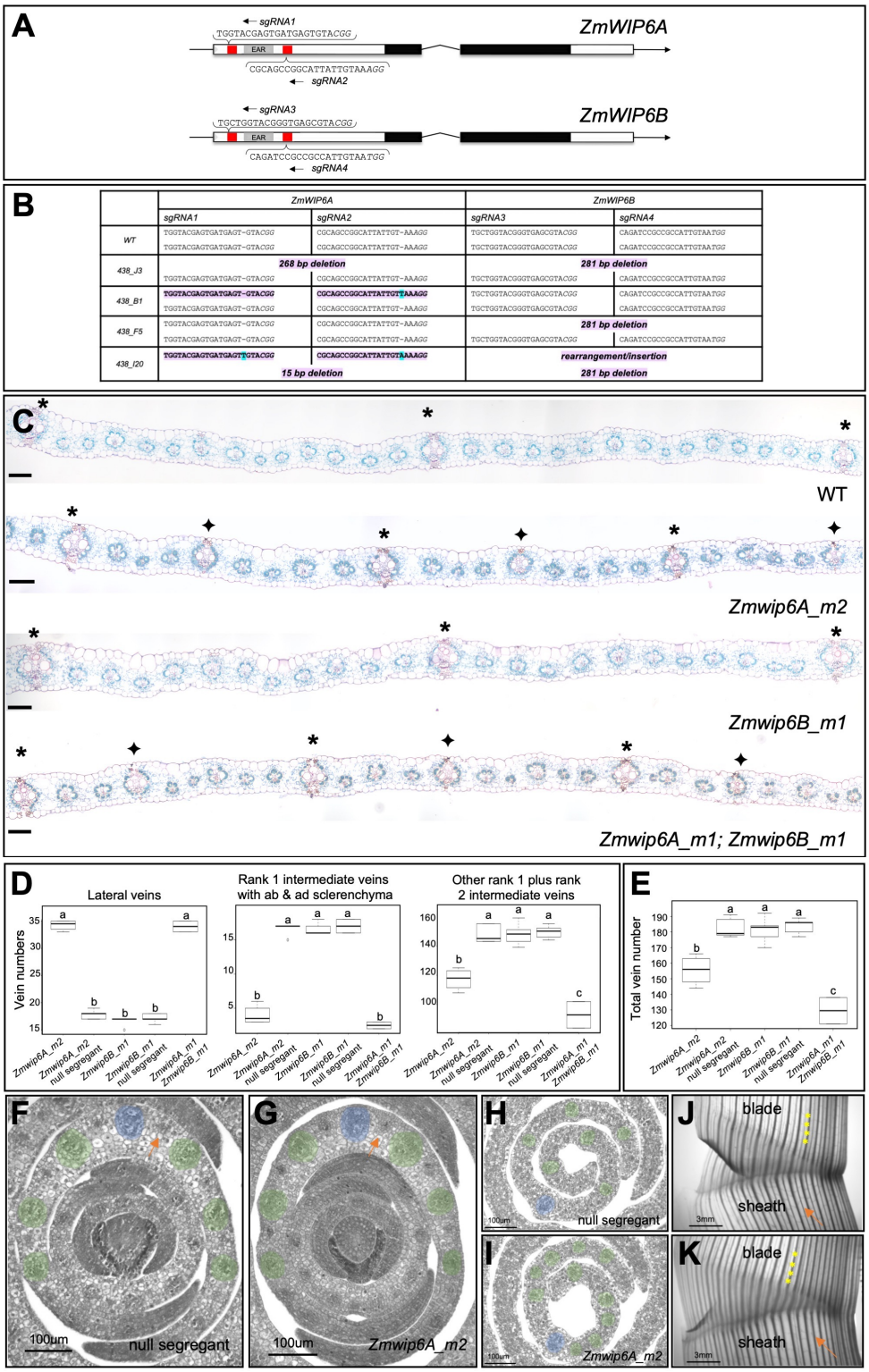

Figure 3. Loss of ZmWIP6A function leads to the formation of too many lateral veins in the maize leaf. A) Gene models of *ZmWIP6A* and *ZmWIP6B* showing 5' and 3' UTRs (black lines) plus two exons (rectangles) separated by an intron (^). The arrow indicates the direction of transcription, the conserved EAR domain (grey box), the C2H2 zinc finger region (black boxes) and the sgRNA target sites (red) are highlighted. The sgRNA sequences used for CRISPR/Cas9 mediated mutagenesis are as shown, with the PAM sequences in italics. **B)** Allelic composition of wild-type (WT) and four T1 maize lines. Mutant alleles are highlighted in pink and base insertions are highlighted in blue. One line (I20) was heteroallelic at both loci, one (J3) was heterozygous at both loci and the other two were heterozygous at one locus and wild-type at the other. **C)** Transverse sections of WT and mutant leaves showing vein numbers and types. In each case samples were taken from the 5th leaf in the region between laterals 2 and 4, with lateral 1 being the closest to the midvein. Asterisks indicate lateral veins, diamonds indicate ectopic lateral veins. Scale bars = 100µm. **D, E)** Quantification of the number of each vein type (D) and of total vein number (E) across the entire medio-lateral axis of the 5th leaf. 'Other rank 1 veins' are those which only have sclerenchyma on the adaxial or abaxial side but not both. N=5 for *Zmwip6B_m1*, *Zmwip6A_m2* null segregant and *Zmwip6B_m1* null segregant, N=4 for *Zmwip6A_m2* and N=2 for the double homozygous *Zmwip6A_m1/Zmwip6B_m1* mutant. Statistical significance was determined using a one way ANOVA followed by a Tukey's test. **F-I)** Transverse sections of null segregant (F, H) and *Zmwip6A_m2* mutant (G, I) P4 primordia at the base (F, G) and in the middle (H, I) of the primordium. Midveins are highlighted in blue and lateral veins (both normal and ectopic) are highlighted in green. Orange arrows point to developing intermediate veins. Scale bars = 100µm. **J, K)** Cleared fragments of leaf 7 stained with Safranin showing the junction of leaf sheath and blade in null segregant (J) and *Zmwip6A_m2* (K) mutant leaves. Orange arrows point to a rank 1 intermediate with abaxial and adaxial sclerenchyma in (J) and an ectopic lateral in the equivalent position in (K). Yellow asterisks are positioned at transverse veins. Scale bar = 3mm

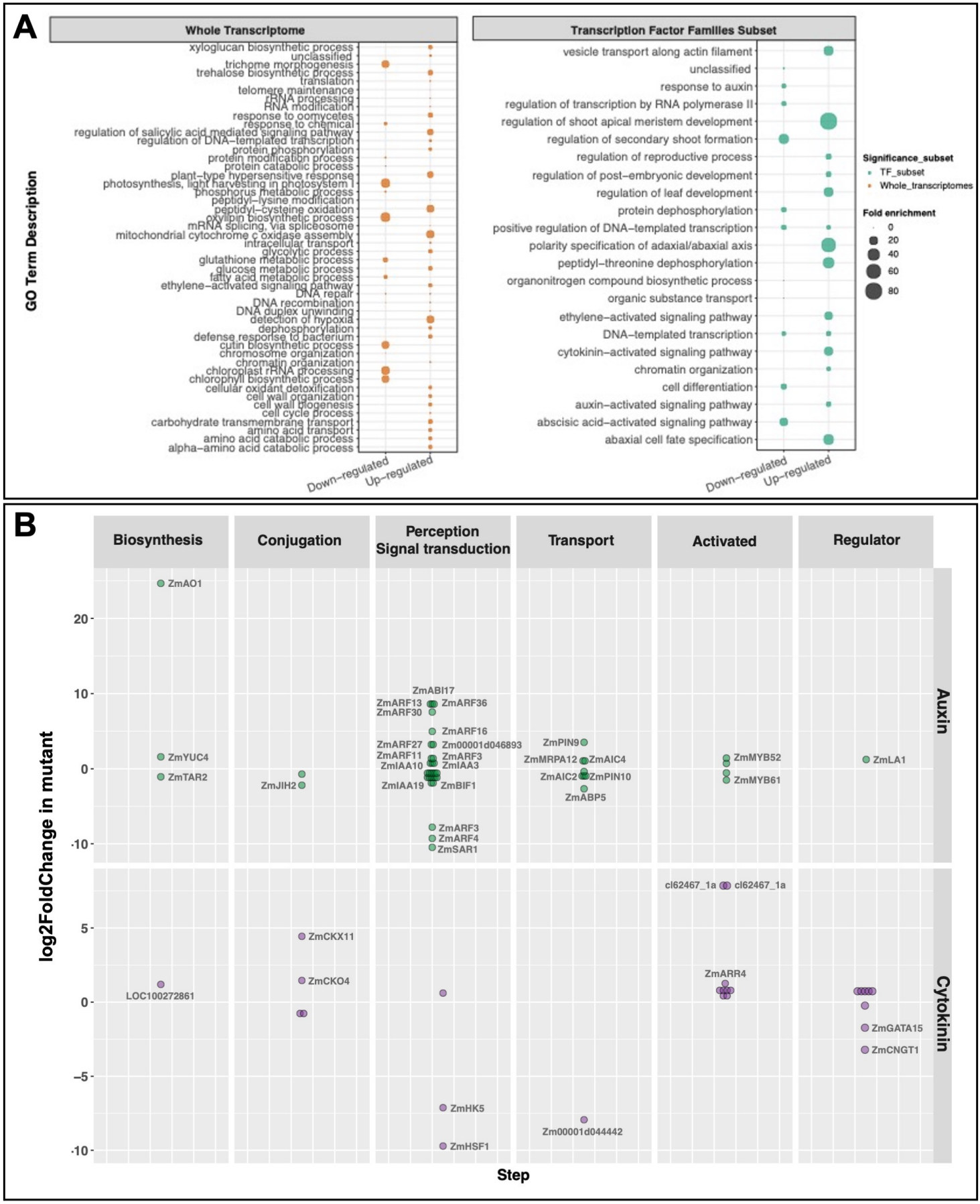

Figure 4. Evidence of auxin and cytokinin pathway perturbations in *Zmtml1tml2* mutant transcriptomes. A) Overrepresentation analysis (ORA) of significantly different transcript levels (L2FC >1; $p \leq 0.05$) in *Zmtml1tml2* mutant apices as compared to corresponding segregating wild-type siblings, using data either from the whole transcriptome or from the subset annotated as transcription factors. Down- and up-regulated components are as indicated and the fold-enrichment in each case is shown by the size of the bubble. **B)** Log2fold difference in levels of transcript encoding auxin and cytokinin pathway components in *Zmtml1tml2* mutant apices as compared to corresponding segregating wild-type siblings. For each pathway step, the genes with significantly different transcript levels (L2FC ± 1; $p \leq 0.05$) are labeled.

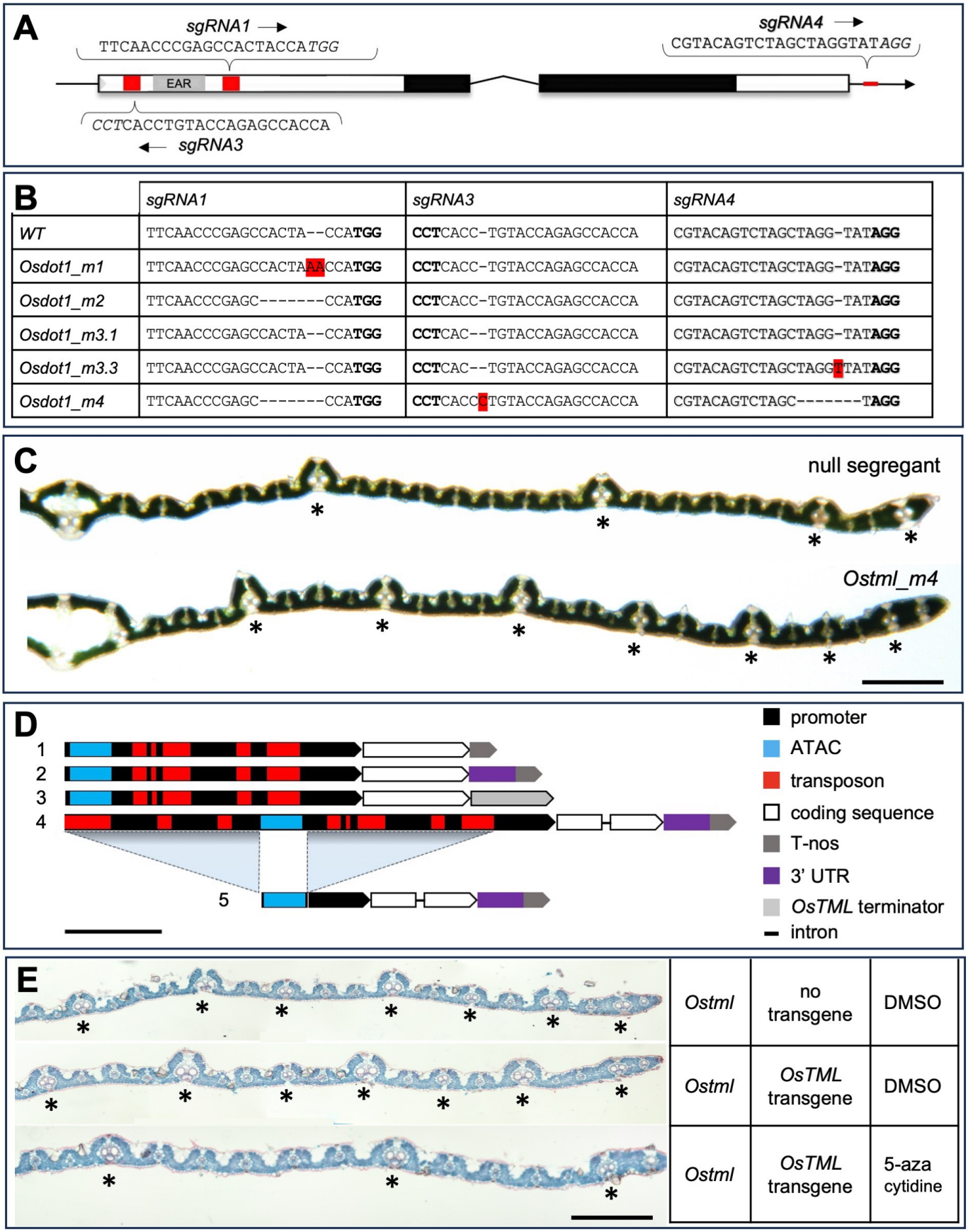

B	sgRNA1	sgRNA3	sgRNA4
WT	TTCAACCCGAGCCACTA--CCA**TGG**	**CCT**CACC-TGTACCAGAGCCACCA	CGTACAGTCTAGCTAGG-TAT**AGG**
Osdot1_m1	TTCAACCCGAGCCACTAAACCA**TGG**	**CCT**CACC-TGTACCAGAGCCACCA	CGTACAGTCTAGCTAGG-TAT**AGG**
Osdot1_m2	TTCAACCCGAGC-------CCA**TGG**	**CCT**CACC-TGTACCAGAGCCACCA	CGTACAGTCTAGCTAGG-TAT**AGG**
Osdot1_m3.1	TTCAACCCGAGCCACTA--CCA**TGG**	**CCT**CAC--TGTACCAGAGCCACCA	CGTACAGTCTAGCTAGG-TAT**AGG**
Osdot1_m3.3	TTCAACCCGAGCCACTA--CCA**TGG**	**CCT**CAC--TGTACCAGAGCCACCA	CGTACAGTCTAGCTAGGTTAT**AGG**
Osdot1_m4	TTCAACCCGAGC-------CCA**TGG**	**CCT**CACCCTGTACCAGAGCCACCA	CGTACAGTCTAGC-------T**AGG**

Figure 5. Ectopic lateral vein formation in *Ostml* mutants of rice cannot be complemented by *OsTML* because transgene expression is suppressed. A) Gene model of *OsTML* showing 5' and 3' UTRs (black lines) plus two exons (rectangles) separated by an intron (^). The arrow indicates the direction of transcription, the conserved EAR domain (grey box), the C2H2 zinc finger region (black boxes) and the sgRNA target sites (red) are highlighted. The sgRNA sequences used for CRISPR/Cas9 mediated mutagenesis are as shown, with the PAM sequences in italics. **B)** Allelic composition of wild-type (WT) and five mutant rice lines. Base insertions are highlighted in red. **C)** Transverse sections of null segregant and *Ostml_m4* mutant leaves (flag leaf minus 1). Asterisks indicate lateral veins. Scale bar = 700 µm. **D)** Schematics of 5 transgenes used to complement *Ostml* mutants. Scale bar = ~1 kb. **E)** Transverse sections of leaf 7 from *Ostml_m3.1* mutant lines that were transformed with construct 2 from (D) and were germinated in the presence or absence of 50 mgL^{-1} 5 aza-cytidine. Asterisks indicate lateral veins. Scale bar = 300 µm.

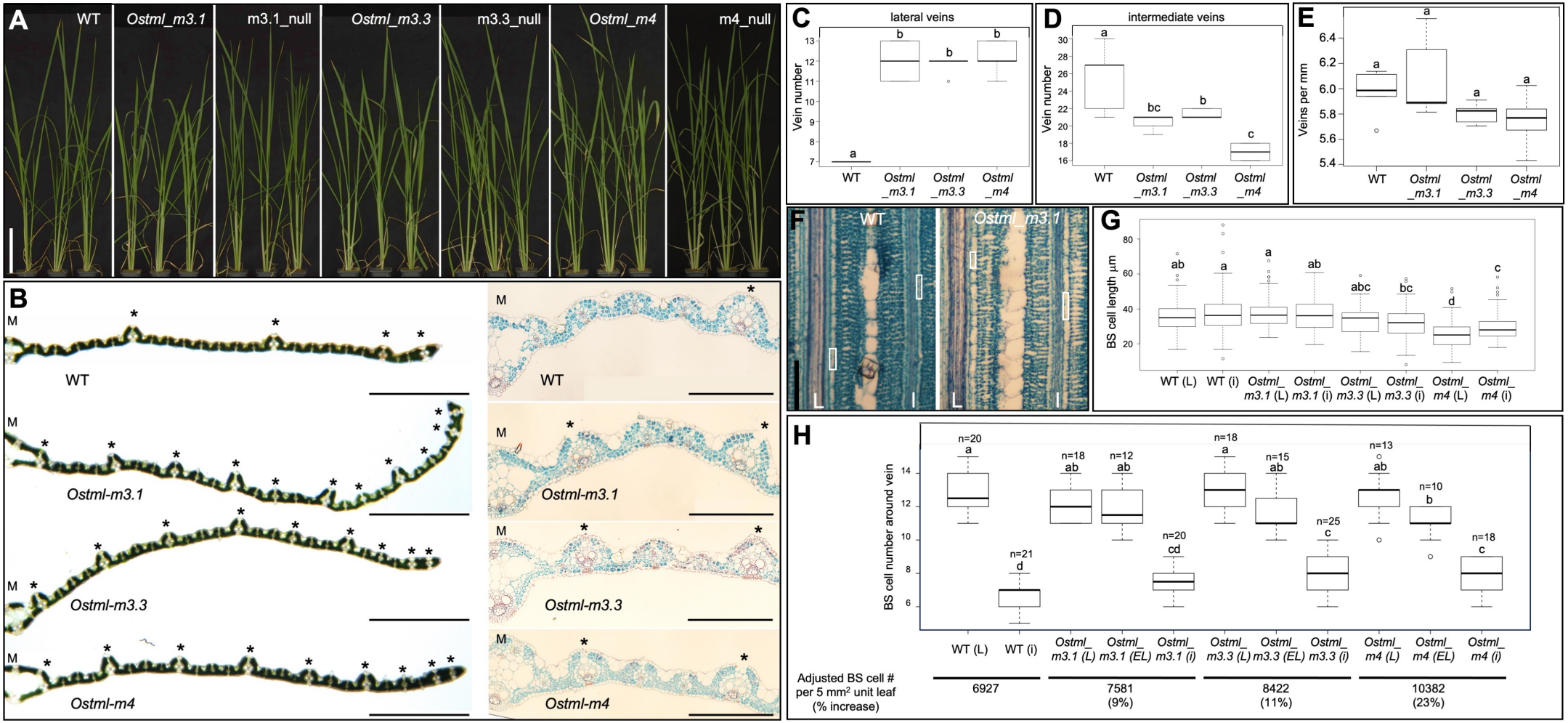

Figure 6. Venation defects in *Ostml* mutant leaves increase total vascular volume and alter bundle sheath cell dimensions. A) Whole plant phenotype of three independent *Ostml* mutant lines and respective null segregant siblings. Lines were selected from F2 populations that had been generated by backcrossing transgene free T1 mutants to Kitaake and then self-pollinating the resultant BCF1 progeny. Scale bar = 10 cm. **B)** Transverse sections imaged between the midvein and the leaf margin of flag leaf minus 1 (left panel) and from the midvein to the position corresponding to the first adjacent lateral vein in wild-type (WT) of leaf 4 (right panel). Asterisks indicate lateral veins. Scale bars = 1 mm (left panel); 200 µm (right panel). **C-E)** Quantification of lateral vein numbers (C), intermediate vein numbers (D) and vein density (E) in leaf 7 of WT and mutant plants. n = 5 for each genotype; different letters indicate statistically different groups as determined using a one-way ANOVA followed by a Tukey's test (p value ≤ 0.05); see Supplementary File 13 for raw data. **F)** Paradermal images of the 7th leaf of WT and mutant plants, imaged in the middle of the blade. Lateral (L) and intermediate (i) veins are indicated. The longest bundle sheath cell around each vein in the field of view is outlined by a white box. Scale bar = 100 µm. **G)** Quantification of bundle sheath cell length around lateral (including ectopic laterals) and intermediate veins of WT and mutant leaves. n = 4 leaf samples and 82/145 cells around L/i veins for WT; 3 leaf samples and 96/114, 45/44 and 130/130 cells for *Ostml_m3.1, _m3,3* and *_m4* mutants respectively. Different letters indicate statistically different groups as determined using a one-way ANOVA followed by a Tukey's test (p value ≤ 0.05); see Supplementary File 13 for raw data. **H)** Quantification of bundle sheath cells numbers around lateral (L), ectopic lateral (EL) and intermediate (i) veins in wild type and mutant plants. Different letters indicate statistically different groups as determined using a one-way ANOVA followed by a Tukey's test (p value ≤ 0.05); see Supplementary File 13 for raw data. Median values for bundle sheath length, number of bundle sheath cells and total vein numbers per leaf were used to estimate total number of bundle sheath cells and percentage increase in number in a leaf unit of 5 mm wide and 1 mm long.

Supplementary Figure 1. WIP6 protein alignment. A, B) Alignment of WIP6 sequences used to infer the phylogenetic tree in Figure 1B (A) and to represent a broader range of species (B). Horizontal lines above the alignment denote the EAR (purple) and WIP (black) domains. Note that sequences in between the EAR and WIP domains do not align across a broad phylogenetic range, although blocks of sequence are conserved within groups e.g. grasses (top box in (B)) and brassicas (bottom box in (B)).

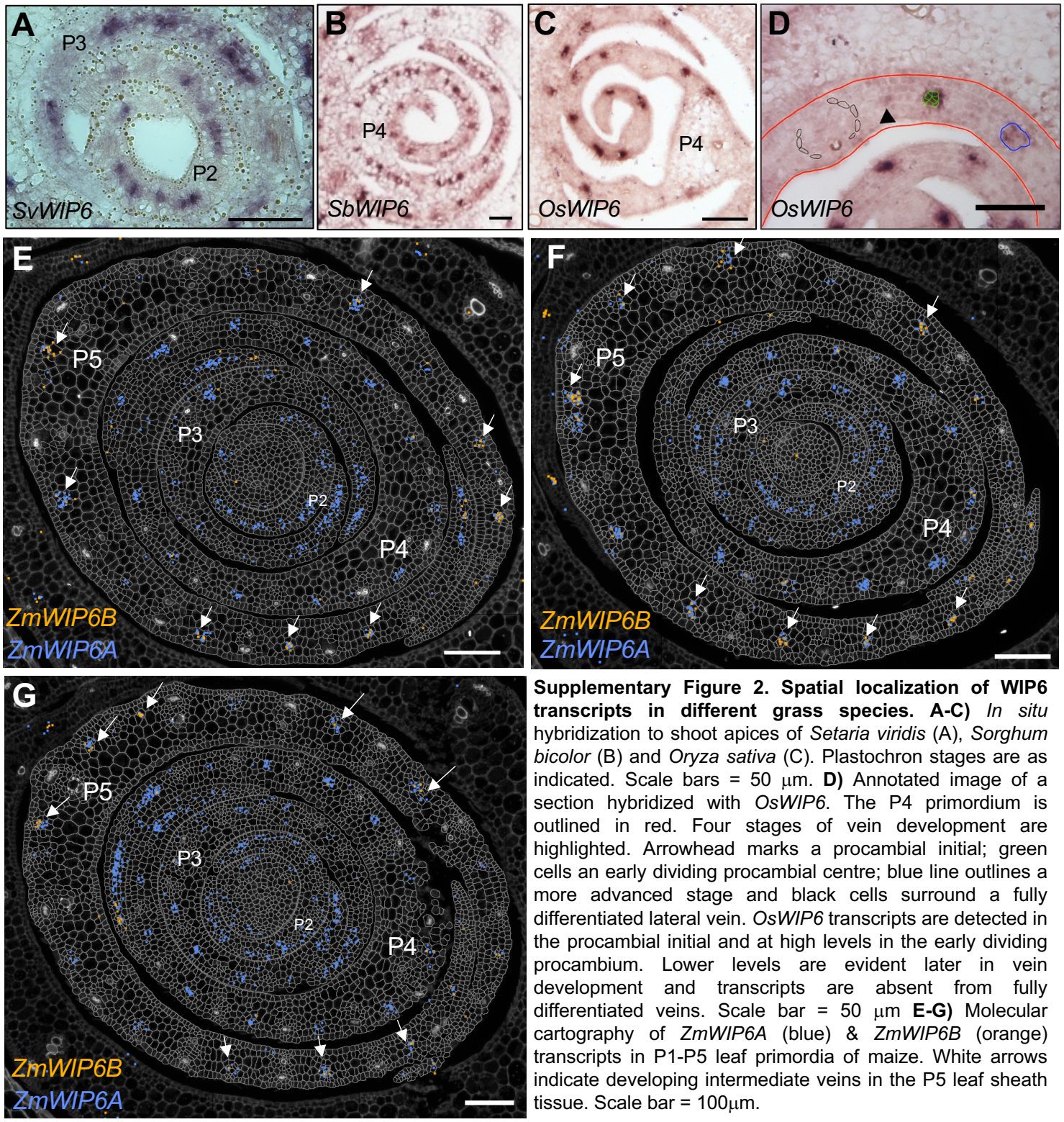

Supplementary Figure 2. Spatial localization of WIP6 transcripts in different grass species. A-C) *In situ* hybridization to shoot apices of *Setaria viridis* (A), *Sorghum bicolor* (B) and *Oryza sativa* (C). Plastochron stages are as indicated. Scale bars = 50 μm. **D)** Annotated image of a section hybridized with *OsWIP6*. The P4 primordium is outlined in red. Four stages of vein development are highlighted. Arrowhead marks a procambial initial; green cells an early dividing procambial centre; blue line outlines a more advanced stage and black cells surround a fully differentiated lateral vein. *OsWIP6* transcripts are detected in the procambial initial and at high levels in the early dividing procambium. Lower levels are evident later in vein development and transcripts are absent from fully differentiated veins. Scale bar = 50 μm **E-G)** Molecular cartography of *ZmWIP6A* (blue) & *ZmWIP6B* (orange) transcripts in P1-P5 leaf primordia of maize. White arrows indicate developing intermediate veins in the P5 leaf sheath tissue. Scale bar = 100μm.

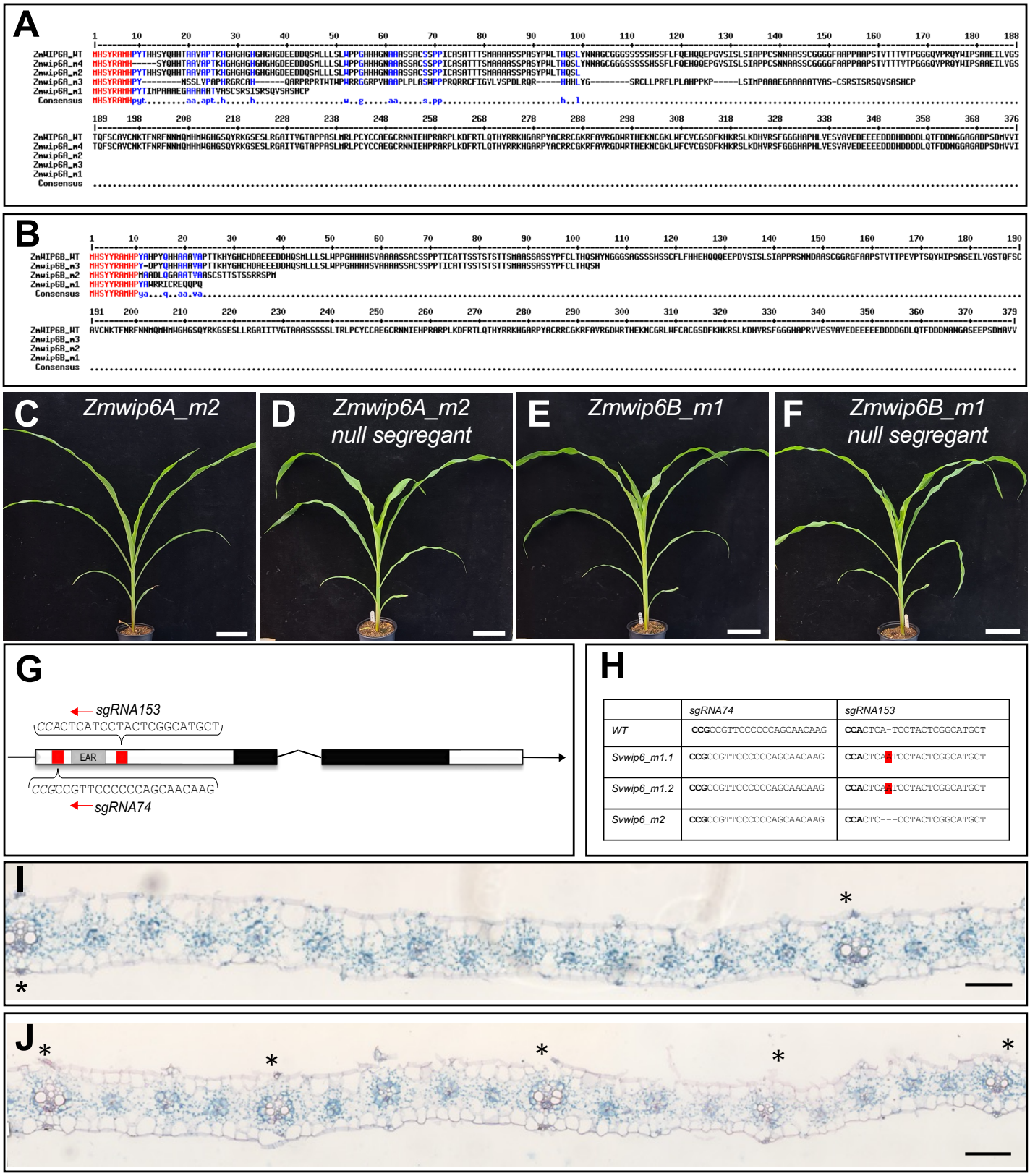

	sgRNA74	sgRNA153
WT	CCGCCGTTCCCCCCAGCAACAAG	CCACTCA-TCCTACTCGGCATGCT
Svwip6_m1.1	CCGCCGTTCCCCCCAGCAACAAG	CCACTCAATCCTACTCGGCATGCT
Svwip6_m1.2	CCGCCGTTCCCCCCAGCAACAAG	CCACTCAATCCTACTCGGCATGCT
Svwip6_m2	CCGCCGTTCCCCCCAGCAACAAG	CCACTC---CCTACTCGGCATGCT

Supplementary Figure 3. WIP6 loss of function alleles in maize and setaria. A, B) Amino acid sequence alignments showing predicted proteins encoded by *Zmwip6A* (A) and *Zmwip6B* (B) mutant alleles. **C-F)** Phenotype of ~one month old *Zmwip6A* mutant (C) and null segregant (D), and *Zmwip6B* (E) mutant and null segregant (F) plants. Scale bar = 10 cm **G)** Gene model of *SvWIP6* showing showing 5' and 3' UTRs (black lines) plus two exons (rectangles) separated by an intron (^). The arrow indicates the direction of transcription, the conserved EAR domain (grey box), the C2H2 zinc finger region (black boxes) and the sgRNA target sites (red) are highlighted. The gRNA sequences used for CRISPR/Cas9 mediated mutagenesis are indicated with the PAM sequence in italics. **H**) Summary of wild-type (WT) and *Svwip6* mutant alleles. **I, J)** Transverse sections of wild-type *S.viridis* and *Svwip6* mutant leaves. Asterisks indicate lateral veins. Scale bar = 100 mm.

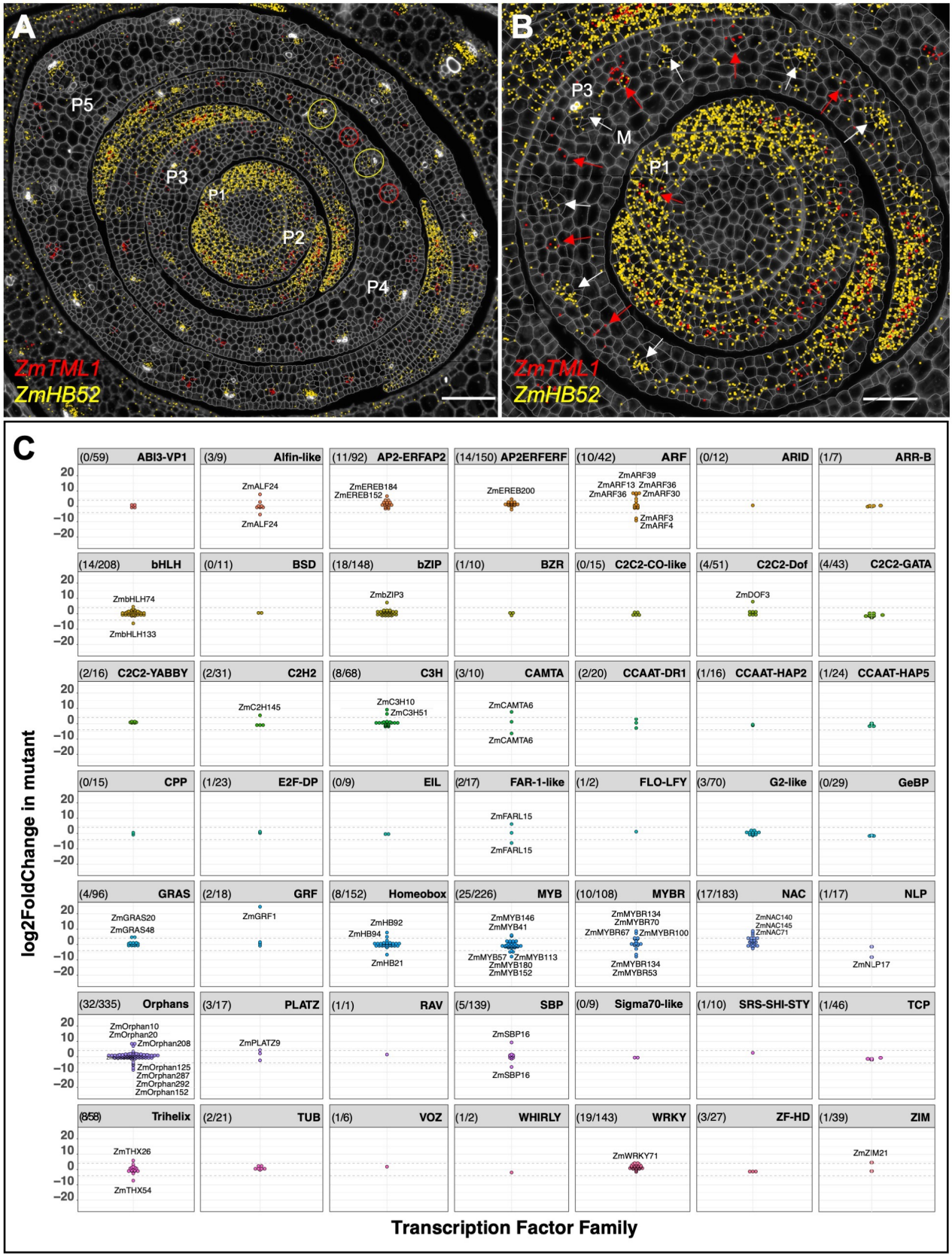

Supplementary Figure 4. Transcription factor expression profiles in maize shoots. A, B) Molecular cartography of *ZmTML1* (red dots) and *ZmHB52* (yellow dots) transcripts in the shoot apical meristem and P1-P5 leaf primordia of wild-type maize apices. Yellow and red circles indicate discrete regions of *ZmHB52* and *ZmTML1* transcript accumulation in differentiated lateral (yellow) and developing intermediate (red) veins of the P4 leaf sheath. White arrows indicate foci of *ZmHB52* transcript accumulation in the P3 primordium at the midvein (M) and at positions where developing procambial centres comprise ~6 cells. Red arrows indicate *ZmTML1* transcript accumulation in the P3 primordium at sites of newly initiated procambial centres that comprise ~1-4 cells. At P1, *ZmHB52* transcripts are detected throughout the primordium whereas *ZmTML1* transcripts are restricted to the developing midvein (red arrow). Scale bars = 100μm (A); 50μm (B). Section is the same as in Figure S2A. **C)** Log2fold difference in levels of transcripts encoding transcription factors in *Zmtml1tml2* mutant apices as compared to corresponding segregating wild-type siblings. For each transcription factor family, the number of genes with significantly different transcript levels (L2FC ± 1; $p \leq 0.05$) between mutant and wild-type is indicated relative to the number of genes in the family in parentheses. Gene names are indicated where more than 4-fold differences were detected.

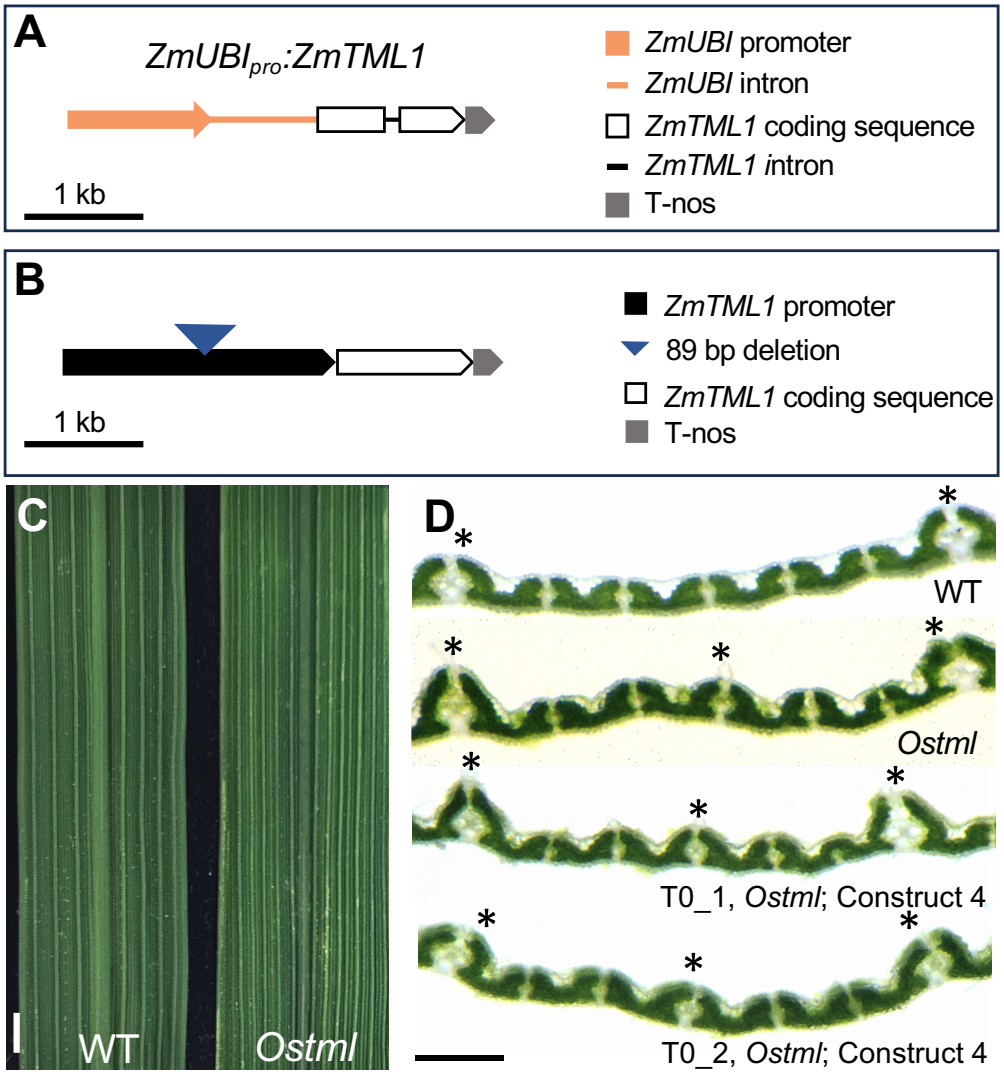

Supplementary Figure 5. Transgenic rice lines expressing *ZmTML* or *OsTML* could not be generated. A) Schematic of construct in which expression of the *ZmTML1* coding sequence was driven constitutively by the maize ubiquitin (*UBI*) promoter. **B)** Schematic of construct used to test *ZmTML1* promoter in rice. **C)** Flag leaf phenotype of wild type and *Ostml* plants showing differences in vein patterns. Scale bar = 2 mm. **D)** Free-hand transverse sections of leaf 7 used to screen transgenic lines in complementation experiments, in this case transformed with complementation construct 4. No complementation was observed in the absence of 5-aza cytidine treatment. Scale bar = 100 µM.

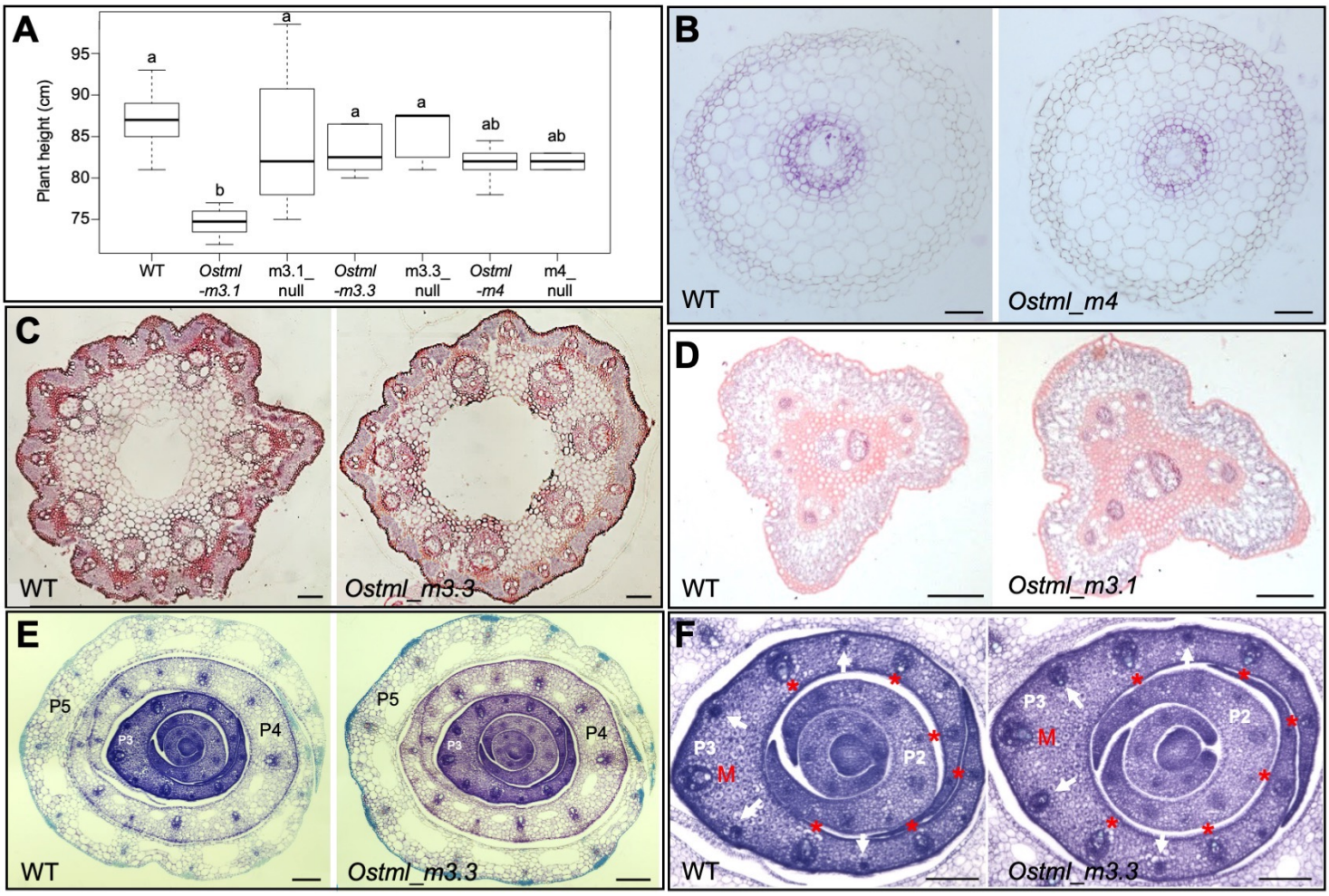

Supplementary Figure 6. Venation defects are restricted to leaves in *Ostml* mutants. A) Quantification of plant height. n ≥ 4; different letters indicate statistically different groups as determined using a one-way ANOVA followed by a Tukey's test (p value ≤ 0.05); see Supplementary File 12 for raw data. **B-D)** Vein patterning is unperturbed in roots (B), rachis (C) and pedicel (D) of *Ostml* mutants. **E, F)** Transverse sections of shoot apices showing the shoot apical meristem and P1-P5 primordia. Venation patterns are indistinguishable in wild-type (WT) and mutant leaf sheaths (visible for P4 and P5 in (E)). In developing leaf blades of P2 and P3 primordia, the size and position of the midrib (M) and lateral veins (red asterisks) are normal but the veins developing at the position of intermediate veins (white arrows) are larger in the mutant (F). Scale bars = 100 µm.

Cloning pOsTML_PU module			
Primer name	**sequence 5'-3'**	**size (bp)**	**modification**
pOsDOT1-A_F	cactctgt**GAAGAC**ttGGAGTGTACATTAAATTTGGGTTGGCA	563	G' to an '**A**'
pOsDOT1-A_R	cactctgt**GAAGAC**ttGTCT**t**GTCCCTCAGCTGG		
pOsDOT1-B_F	cactctgt**GAAGAC**ttAGACCGGGGGAGGAGAGG	388	T' to an '**A**'
pOsDOT1-B_R	cactctgt**GAAGAC**ttAGGGAGAG**t**CCGGTGGTTATAT		
pOsDOT1-C_F	cactctgt**GAAGAC**ttCCCTCTCTCATCTTGTCGTG	1329	none
pOsDOT1-C_R	TCTC**GAAGAC**TGTGTCGAAGT		
pOsDOT1-D_F	cactctgt**GAAGAC**ttGACACAGTC**a**TCGAGATACTACTT	810	T' to an '**A**'
pOsDOT1-D_R	cactctgt**GAAGAC**ttCATTGCTCTGTACCTGCTGCTG		
Cloning OsTML_T module			
DOT1_3'term GG-F	cactctg**tGAAGAC**ttGCTTCTTAATTATTTTGTGTTTAATTAATTAC	843	none
DOT1_3'term GG-R	cactctgt**GAAGAC**ttAGCGTCTTTCAAGTTCAATGCAAA		
Cloning 3'UTROsTML+TNOS_T module			
DOT1_3'term GG-F	cactctgt**GAAGAC**ttGCTTCTTAATTATTTTGTGTTTAATTAATTAC	458	none
DOT1_3'UTR- R	AAAACGGAGGAAGTATGTGT		
tNOS-F	GTCAAGCAGATCGTTCAAAC	263	none
tNOS-R	cactctgtGAAGACttAGCGTCGATCTAGTAACATAGATGACAC		
Cloning OsTML genomic clone using NEBuilder HiFi DNA Assembly			
pOsDOT1g-1F	aacggatcacttcgtgtcccACAGGGCATGCTTCTAGGTT	3400	none
OsDOT1g-3R	TCCGTACTAGGGATATGTCTCA		
OsDOT1g-4F	TGAGACATATCCCTAGTACGGA	1849	none
OsDOT1g-5R	TGAGTGAGAGAGTTTGGAAGGT		
OsDOT1del_F	ACCTTCCAAACTCTCTCACTCA	1533	none
OsDOT1del_R	CTGCCTAGCCTAGCCATCTA		
OsDOT1g-6F	TAGATGGCTAGGCTAGGCAG	595	none
tNOS-R_Gibson	tcacgctgcactgcagctccTCGATCTAGTAACATAGATGACAC		
Cloning OsTMLgATAC clone using NEBuilder HiFi DNA Assembly			
pOsDOT1-ATAC_F	ctgtcaaacactgatagtttTGAGATGAAGGAAATAGGTCA	540	none
pOsDOT1-ATAC_R	agaatatgtgttatttagtgcTCCGTACTAGGGATATGTCTCA		

Supplementary Table 1. Primer sequences used for cloning the *OsTML* complementation constructs. Domestication of the BsaI/BpiI enzyme recognition sites was done by introducing base pair changes listed under "modification". The BpiI sites used for assembling the fragments into a Level 0 OsTML PU module are marked in bold. Primers for the NEBuilder assembly carry 20 bp primer extensions (lower case) to allow seamless integration into the destination vector.